ARF6–JIP3/4 regulate endosomal tubules for MT1-MMP exocytosis in cancer invasion

Valentina Marchesin,[1,6,7]* Antonio Castro-Castro,[1,6]* Catalina Lodillinsky,[1,6] Alessia Castagnino,[1,6] Joanna Cyrta,[1,6] Hélène Bonsang-Kitzis,[2,3,4] Laetitia Fuhrmann,[5] Marie Irondelle,[1,6] Elvira Infante,[1,6] Guillaume Montagnac,[1,6] Fabien Reyal,[2,3,4] Anne Vincent-Salomon,[5] and Philippe Chavrier[1,6]

[1]PSL Research University, [2]Department of Translational Research, Residual Tumor and Response to Treatment Laboratory, [3]Institut National de la Sante et de la Recherche Médicale, Unite Mixte de Recherche 932 Immunity and Cancer, [4]Department of Surgery, and [5]Department of Pathology, Institut Curie, 75248 Paris, France
[6]Membrane and Cytoskeleton Dynamics, Centre National de la Recherche Scientifique, Unite Mixte de Recherche 144, 75248 Paris, France
[7]University Pierre et Marie Curie Paris 06, 75000 Paris, France

Invasion of cancer cells into collagen-rich extracellular matrix requires membrane-tethered membrane type 1–matrix metalloproteinase (MT1-MMP) as the key protease for collagen breakdown. Understanding how MT1-MMP is delivered to the surface of tumor cells is essential for cancer cell biology. In this study, we identify ARF6 together with c-Jun NH_2-terminal kinase–interacting protein 3 and 4 (JIP3 and JIP4) effectors as critical regulators of this process. Silencing ARF6 or JIP3/JIP4 in breast tumor cells results in MT1-MMP endosome mispositioning and reduces MT1-MMP exocytosis and tumor cell invasion. JIPs are recruited by Wiskott-Aldrich syndrome protein and scar homologue (WASH) on MT1-MMP endosomes on which they recruit dynein–dynactin and kinesin-1. The interaction of plasma membrane ARF6 with endosomal JIPs coordinates dynactin–dynein and kinesin-1 activity in a tug-of-war mechanism, leading to MT1-MMP endosome tubulation and exocytosis. In addition, we find that ARF6, MT1-MMP, and kinesin-1 are up-regulated in high-grade triple-negative breast cancers. These data identify a critical ARF6–JIP–MT1-MMP–dynein–dynactin–kinesin-1 axis promoting an invasive phenotype of breast cancer cells.

Introduction

The ability of tumor cells to invade surrounding tissue and disseminate to distant sites is one hallmark of cancer and a predominant cause of cancer-related death. One intrinsic property of metastatic tumor cells is their ability to degrade components of the ECM and thereby breach tissue barriers. ECM remodeling by cancer cells is executed by matrix-degrading proteases (Bonnans et al., 2014). Membrane-tethered membrane type 1–matrix metalloproteinase (MT1-MMP) is overexpressed by carcinoma cells of various origins and is a critical mediator of the pericellular matrix remodeling required for invasive tumor growth and metastasis (Hotary et al., 2003, 2006; Lodillinsky et al., 2015).

Surface levels of MT1-MMP increase during breast tumor progression, particularly in targeted therapy-lacking triple-negative breast cancers (TNBCs; Lodillinsky et al., 2015). In TNBC cell lines, newly synthesized MT1-MMP reaches the plasma membrane and is rapidly internalized (Poincloux et al., 2009). Internalized MT1-MMP accumulates in late endocytic compartments from where it is delivered to invadopodia, corresponding to specialized plasma membrane–matrix contact sites involved in pericellular matrix proteolysis (Steffen et al., 2008; Williams and Coppolino, 2011; Yu et al., 2012; Hoshino et al., 2013; Monteiro et al., 2013). Delivery of MT1-MMP to invadopodia requires tubular membrane connections forming between MT1-MMP–containing late endosomes (LEs) and the invadopodial plasma membrane (Monteiro et al., 2013). This mechanism requires MT1-MMP–containing endosomes to be transported to the cell periphery toward invadopodia (Steffen et al., 2008; Yu et al., 2012; Monteiro et al., 2013). Along this line, trafficking of MT1-MMP involves microtubules and microtubule plus end–directed kinesin motors in human macrophages (Wiesner et al., 2010).

LEs exhibit bidirectional motility as a result of a tug of war between dynein–dynactin and kinesin motors in opposite directions (Granger et al., 2014). The direction of endosome movement can be controlled by motor adapter proteins, including JNK-interacting protein 3 and 4 (JIP3 and JIP4), which bind to kinesin-1 and dynactin (Bowman et al., 2000; Cavalli et al.,

*V. Marchesin and A. Castro-Castro contributed equally to this paper.

Correspondence to Philippe Chavrier: philippe.chavrier@curie.fr

Abbreviations used in this paper: CCD, charge-coupled device; CMV, cytomegalovirus; DCIS, ductal carcinoma in situ; DIC, differential interference contrast; ER, estrogen receptor; IDC, invasive ductal carcinoma; IF, immunofluorescence; IHC, immunohistochemistry; IP, immunoprecipitate; JIP, JNK-interacting protein; LE, late endosome; MT1-MMP, membrane type 1–matrix metalloproteinase; PCR, polymerase chain reaction; PLA, proximity ligation assay; PR, progesterone receptor; TIRF, total internal reflection fluorescence; TMA, tissue microarray; TNBC, triple-negative breast cancer; WASH, Wiskott-Aldrich syndrome protein and scar homologue; WD, working distance.

The Rockefeller University Press $30.00
J. Cell Biol. Vol. 211 No. 2 339–358
www.jcb.org/cgi/doi/10.1083/jcb.201506002

2005; Montagnac et al., 2009; Sun et al., 2011). The switching of JIP3/JIP4 between kinesin-1 and dynactin–dynein on recycling endosomes is regulated by the small GTPase ARF6, which binds JIP3/JIP4 in its GTP-bound activated form (Montagnac et al., 2009). A large body of work implicates ARF6 in the motile phenotype and metastatic potential of cancer cells (D'Souza-Schorey and Chavrier, 2006). Overexpression of ARF6 correlates with increased matrix invasion activity of melanoma and breast tumor–derived cell lines (Hashimoto et al., 2004; Tague et al., 2004). A pathway consisting of ARF6, the ARF6 guanine exchange factor GEP100/BRAG2, and AMAP1 (DDEF1 or ASAP1), an ARF6 downstream effector, promotes tumor invasion and metastasis in breast cancer in response to epidermal growth factor receptor activation (Morishige et al., 2008; Sabe et al., 2009).

In this study, we analyzed the contribution of ARF6 and JIP3/JIP4 effector proteins to the trafficking of MT1-MMP in breast cancer cells. We found that JIP3/JIP4 control the recruitment of dynactin–dynein and kinesin-1 motor proteins on MT1-MMP–positive endosomes, whereas kinesin-2 recruitment is independent of JIPs. Through interaction with endosomal JIP3/JIP4, plasma membrane ARF6 opposes dynactin–dynein-dependent movement of MT1-MMP endosomes, promoting endosomal membrane tubulation by kinesin-1 and the transfer of MT1-MMP to the plasma membrane. JIP recruitment to MT1-MMP endosomes requires endosomal Arp2/3 complex activator Wiskott-Aldrich syndrome protein and scar homologue (WASH), suggesting coordination of actin-based tubular membrane deformation and microtubule-dependent pulling force generation for endosomal membrane tubule formation. Immunohistochemistry (IHC) analysis of invasive breast tumor specimens revealed a coup regulation of KIF5B kinesin-1 subunit, MT1-MMP, and plasma membrane ARF6 in high-grade TNBCs identifying an MT1-MMP–ARF6–JIP3/JIP4–kinesin-1 axis in breast cancer invasion.

Results

ARF6 is required for matrix remodeling and invasive migration by TNBC cell lines

ARF6 silencing was assessed in MDA-MB-231 cells, classified as highly invasive TNBC (Neve et al., 2006). Confirming earlier studies (Hashimoto et al., 2004; Tague et al., 2004), silencing of ARF6 by siRNAs (Fig. S1, A and C) decreased FITC-gelatin degradation by 60% as compared with cells treated with nontargeting siRNA (siNT; Fig. 1 A). MT1-MMP knockdown almost completely abolished gelatin degradation by MDA-MB-231 cells (Fig. 1 A and Fig. S1 B). ARF6 knockdown did not interfere with MT1-MMP expression (Fig. S1, A and C). We also investigated the consequence of ARF6 silencing on the capacity of breast cancer cells to invade in a 3D type I collagen matrix over a 2-d period. As compared with multicellular spheroids of MDA-MB-231 cells treated with siNT, invasion by ARF6-depleted spheroids was decreased by ∼40%, similar to MT1-MMP–knocked down spheroids (Fig. 1, B and C; and Fig. S1 D).

The generality of ARF6's contribution to the invasive potential was assessed in MCF10DCIS.com cells, which generate ductal carcinoma in situ (DCIS)–like lesions and require MT1-MMP for invasion (Hu et al., 2008; Lodillinsky et al., 2015). Similar to the situation in MDA-MB-231 cells, knockdown of ARF6 or MT1-MMP (Fig. S1 E) led to a 50% decrease in the invasion capacity of MCF10DCIS.com multicellular spheroids in type I collagen (Fig. S1, F and G). We then sought to investigate whether inhibition of cell invasion resulted from a requirement for ARF6 in TNBC's ability to proteolytically cleave surrounding collagen fibers. We used the neoepitope Col1-$^{3/4}$C antibody, which recognizes the collagenase-cleaved fragment of collagen I (Wolf et al., 2007; Monteiro et al., 2013). In MDA-MB-231 cells embedded in type I collagen, depletion of MT1-MMP strongly reduced pericellular collagen degradation as indicated by a 70% reduction of Col1-$^{3/4}$C antibody signal (Fig. 1, D and E). Thus, collagen degradation by MDA-MB-231 cells strongly relies on MT1-MMP activity. Silencing of ARF6 led to a similar decrease of collagen proteolysis (Fig. 1, D and E), suggesting that ARF6 is implicated in MT1-MMP–dependent pericellular collagen degradation. Altogether, these data indicate a requirement for ARF6 in matrix remodeling and in the invasive potential of TNBC cells.

JIP3 and JIP4 are required for invasive migration through 3D type I collagen

We initially identified the related JIP3 and JIP4 proteins as ARF6 downstream effectors controlling microtubule-based endosome movement through regulation of kinesin-1 and the dynactin–dynein complex (Isabet et al., 2009; Montagnac et al., 2009), suggesting a possible role for ARF6–JIP3/JIP4 in microtubule-dependent movement of MT1-MMP–positive endosomes. JIP3 and JIP4 expression was detected by immunoblotting analysis in MDA-MB-231 cells (Fig. S2, A and B). Immunofluorescence (IF) staining revealed a cytosolic diffuse distribution and a punctate association with the cytosolic face of cytoplasmic vesicles; most of these vesicles were positive for MT1-MMPmCherry (MT1-MMPmCh; Fig. 2 A; Sakurai-Yageta et al., 2008). Staining was abolished by JIP4 silencing (Fig. S2 C). JIP3 could not be detected due to a lack of IF-grade antibodies. The contribution of JIP3 and JIP4 to the invasive potential of MDA-MB-231 cells was analyzed. Knockdown of JIP3 or JIP4 led to a significant decrease of FITC-gelatin degradation (Fig. S2 D) and invasion of multicellular spheroids in 3D type I collagen (Fig. 2 B and Fig. S2 E). Double knockdown of JIP3 and JIP4 using two independent pairs of siRNAs resulted in a similar inhibition of invasion, suggesting a mutually dependent function of the two proteins (Fig. 2 C and Fig. S2 F). Moreover, the requirement for JIP3 and JIP4 in invasive migration was paralleled by a 50–65% decrease in the capacity of JIP3/JIP4-depleted cells to cleave type I collagen (Fig. 2 D and Fig. S2 G). Thus, together with ARF6, our data identify JIP3 and JIP4 as important components of the matrix remodeling and invasion program of MDA-MB-231 breast tumor cells.

The ARF6–JIP pathway controls MT1-MMP–positive endosome positioning and exocytosis

VAMP7- and Rab7-positive LEs represent a major reservoir of MT1-MMP involved in exocytosis and surface delivery of the protease to support pericellular matrix proteolysis (Steffen et al., 2008; Williams and Coppolino, 2011; Yu et al., 2012; Hoshino et al., 2013; Monteiro et al., 2013). The capacity of ARF6 and JIPs to control the distribution of MT1-MMP–positive LEs was assessed. Automated image analysis of the endosome position showed that MT1-MMPmCh accumulated in large, centrally located endosomes and smaller, more dispersed endosomal compartments (siNT; Fig. 2 E, blue curve; and Fig. 2 F) with

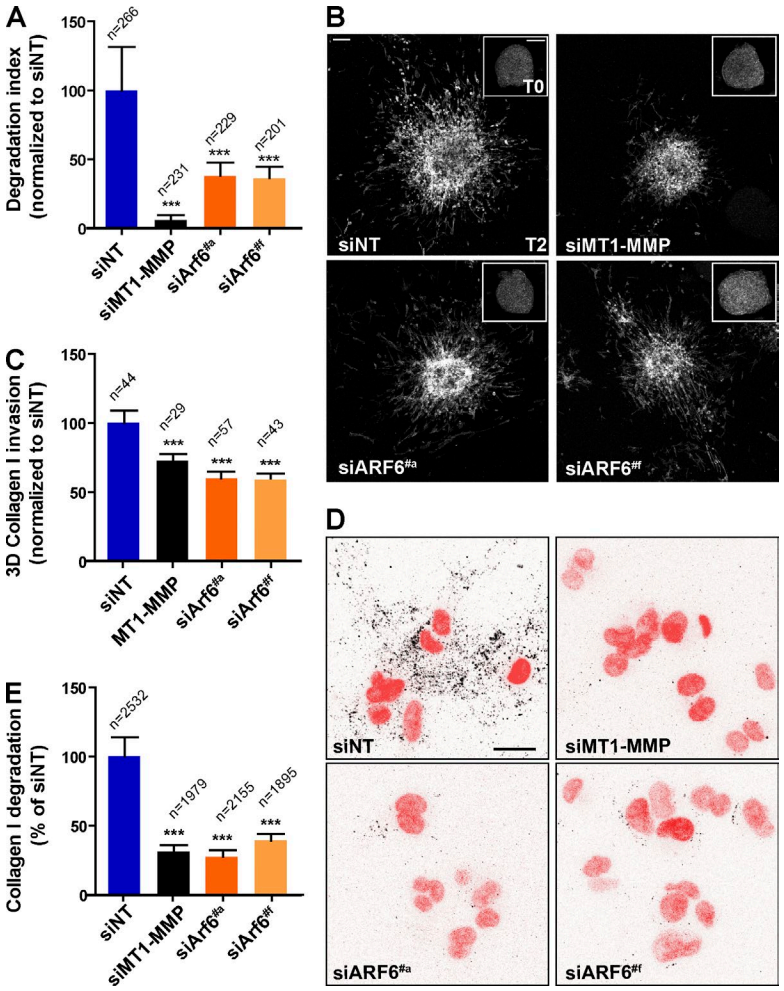

Figure 1. **ARF6 is required for matrix degradation and invasive migration of breast tumor cells through 3D type I collagen.** (A) FITC-gelatin degradation. *n*, number of cells scored for each cell population treated with indicated siRNAs. ***, $P < 0.001$ (compared with siNT-treated cells). (B) Phalloidin-labeled MDA-MB-231 cell spheroids after 2 d in 3D collagen I (T2). Insets show spheroids immediately after embedding in collagen (T0). Bars, 200 µm. (C) Mean invasion area of spheroids at T2 normalized to mean spheroid area at T0 and to invasion of siNT spheroids set to 100 ± SEM. *n*, spheroid number. ***, $P < 0.001$. (D) MDA-MB-231 cells treated with indicated siRNAs embedded in collagen I and stained for cleaved collagen with Col1-$^{3/4}$C antibody (black in the inverted image). DAPI-stained nuclei are shown in red. Bar, 20 µm. (E) Collagenolysis by MDA-MB-231 cells (Col1-$^{3/4}$C antibody signal as in D). Values are mean normalized degradation index ± SEM. *n*, number of cells analyzed for each cell population. ***, $P < 0.001$ (as compared with siNT-treated cells).

a strong overlap with Rab7 late endocytic marker (Fig. S3, A and C; Steffen et al., 2008; Monteiro et al., 2013). Analysis of vesicle movement by color coding the maximum intensity time projection of selected frames from time-lapse sequences revealed highly dynamic bidirectional movement of MT1-MMP–positive endosomes (Fig. 2 F, inset 1; and Video 1). Silencing of ARF6 with three independent siRNAs led to a dramatic redistribution and clustering of MT1-MMP–positive endosomes to the central cell region (Fig. 2 E, orange and brown curves; and Fig. 2 F), where these large vacuolar structures remained essentially static (appearing as white in a color-coded representation of movement; Fig. 2 F, inset 2; and Video 1). However, JIP3/JIP4 double–knocked down cells had a more dispersed distribution of MT1-MMP endosomes (Fig. 2 E, green curve) and accumulated clusters of MT1-MMP–positive vesicles at the cell periphery, which were mostly nonmotile (Fig. 2 F, insets 3–5; and Video 1). Knockdown of ARF6 or JIP did not affect MT1-MMP and Rab7 overlap (Fig. S3, A and C) nor limited colocalization with EEA1-positive early endosomal compartments (Fig. S3, B and C), indicating that loss of ARF6 or JIP function affected the steady-state distribution of Rab7/MT1-MMP–positive LEs with minimal effect on endosomal cargo sorting and/or endosome maturation. The N-terminal region of JIP3 and JIP4 contains two leucine zipper (LZI and LZII) domains known to mediate dimerization of the proteins (Kelkar et al., 2000; Nguyen et al., 2005; Isabet et al., 2009). As an alternative approach to interfere with JIP3/JIP4 dimerization and inhibit their function, we overexpressed the LZ1 domain of JIP3 (aa 1–266). JIP3-LZI induced the redistribution of MT1-MMP endosomes to the cell periphery similar to JIP3/JIP4 silencing (Fig. 2 G, light green). In contrast, expression of GFP or a variant JIP3-LZI domain with two leucine to proline substitutions (LZI/L83P-L89P) abolishing dimerization (not depicted) did not affect MT1-MMP localization (Fig. 2 G, dark green).

As surface MT1-MMP is directly responsible for pericellular matrix degradation, we investigated the role of ARF6 and JIP3/JIP4 in MT1-MMP exocytosis from LEs in relation to their identified function in endosome positioning. MDA-MB-231 cells expressing MT1-MMPpHluorin were cultured on fibrillar type I collagen, and we monitored the apparition of green fluorescence flashes corresponding to dequenching of the fluorescence of the extracellular pHluorin tag upon exocytosis of MT1-MMP–positive LEs (Monteiro et al., 2013). As previously reported (Monteiro et al., 2013), exocytic events occurred mainly in association with collagen I fibers and led to surface accumulation of MT1-MMP along ECM fibers (Fig. S3 D). Quantification of MT1-MMPpHluorin flashes revealed a decrease in frequency of MT1-MMP exocytic events upon ARF6 or JIP3/4 knockdown (Fig. S3 E). Therefore, mispositioning of MT1-MMP–containing LEs as a consequence of ARF6 or JIP3/JIP4 loss of function correlated with impaired MT1-MMP exocytosis. Altogether, we conclude that defects in matrix remodeling and invasive migration correlate with dramatic and opposite changes in the distribution of

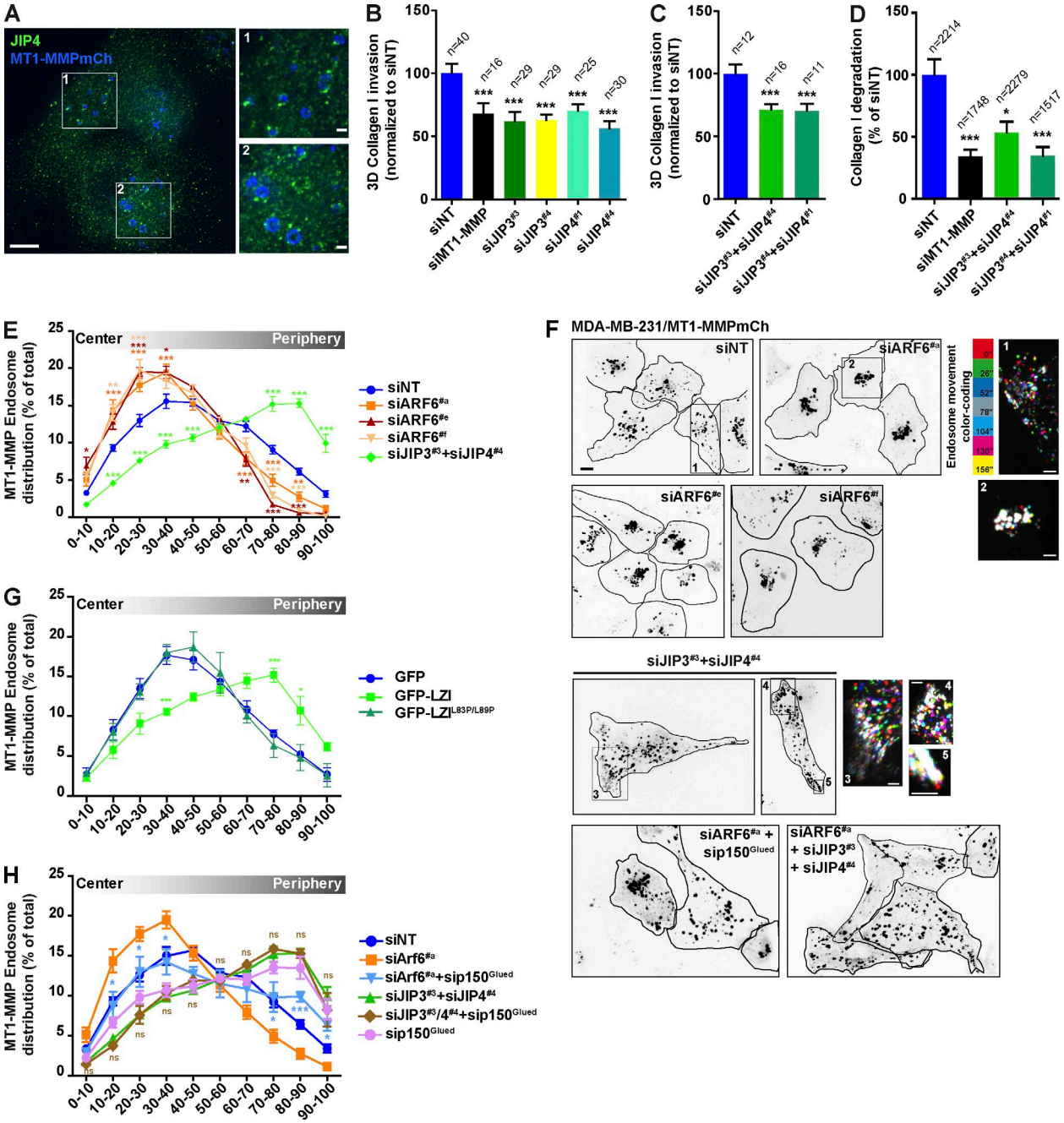

Figure 2. **Regulation of MT1-MMP–positive endosome positioning by ARF6 and JIP3/JIP4.** (A) JIP4 staining of MT1-MMPmCh–expressing MDA-MB-231 cells. Bars: 5 µm; (insets) 2 µm. (B and C) Mean invasion area of multicellular spheroids after 2 d in 3D collagen normalized to mean spheroid area at T0 and to invasion of siNT-treated spheroids set to 100 ± SEM. *n*, spheroids number. ***, P < 0.001. (D) Collagenolysis by MDA-MB-231 cells treated with the indicated siRNAs. Values are mean normalized degradation index ± SEM. *n*, number of cells analyzed for each cell population. *, P < 0.05; ***, P < 0.001 (as compared with siNT-treated cells). (E) Distribution of MT1-MMPmCh endosomes in MDA-MB-231 cells plated on 2D gelatin. Mean percentage of MT1-MMP–positive endosomes according to their cell center-to-cell periphery position ± SEM. **, P < 0.01; ***, P < 0.001 (compared with siNT distribution). (F) Inverted still images from time-lapse sequences of MDA-MB-231 cells expressing MT1-MMPmCh treated with indicated siRNAs (see Video 1). Insets show color-coded time projections of selected time frames from these sequences (color code shown on the left of inset 1) corresponding to the boxed regions at higher magnification. Bars: 10 µm; (insets) 5 µm. (G) Distribution of MT1-MMPmCh endosomes in MDA-MB-231 cells expressing the indicated JIP3-LZI construct as in E. (H) MT1-MMPmCh endosome distribution as in E. *, P < 0.05; ***, P < 0.001 with siARF6+sip150Glued as compared with siARF6 treatment and siJIP3/4+sip150Glued as compared with siJIP3/4. ns, not significant.

MT1-MMP–positive LEs in MDA-MB-231 cells depleted for ARF6 or JIP3/JIP4, respectively. These effects culminate in a decrease in MT1-MMP exocytosis at the surface and inhibition of pericellular matrix degradation and correlate with reduced invasive potential of TNBCs.

Regulation of MT1-MMP endosome position by ARF6 requires JIP3/JIP4 and p150Glued dynactin complex subunit

Perinuclear clustering of MT1-MMP–positive endosomes could indicate unbalanced dynactin–dynein minus end–directed

motor activity in ARF6-depleted MDA-MB-231 cells. Along this line, knockdown of the dynactin complex subunit p150^{Glued} (Fig. S3 F) induced a more dispersed and peripheral distribution of MT1-MMP endosomes (Fig. 2 H, pink curve). In epistasis experiments, p150^{Glued} knockdown restored a normal-like distribution of MT1-MMP endosomes in ARF6-depleted cells as compared with perinuclear clustering in cells depleted for ARF6 only (Fig. 2, F and H, compare light blue with orange curve; and Fig. S3, F and G). Thus, loss of ARF6 seems to favor dynein function. Similarly, depletion of ARF6 and JIP3/JIP4 together also reverted si-ARF6–mediated perinuclear MT1-MMP endosome clustering and led to the accumulation of endosomes at the cell periphery (Fig. 2, F and H, compare brown with orange curve), indicating a requirement for JIP3/JIP4 function in the regulation of endosome positioning by ARF6 through control of the dynein–dynactin complex function. Finally, double p150^{Glued} and JIP3/JIP4 knockdown resulted in a scattered and peripheral distribution of MT1-MMP–positive endosomes as in the single knockdown of each protein (Fig. 2 H, compare brown with green or pink curve; and Fig. S3 H), supporting the conclusion that JIPs and the dynactin complex work within the same pathway.

Kinesin-1 and kinesin-2 are required for MT1-MMP endosome movement

Association of kinesin-1 (KIF5B), kinesin-2 (KIF3A), and p150^{Glued} dynactin complex subunit with MT1-MMP–containing endosomes was assessed at an endogenous level by double-labeling IF analysis and 3D deconvolution microscopy. Specificity of antibodies to p150^{Glued}, KIF5B, and KIF3A was demonstrated by a loss of staining in cells silenced for these proteins (Fig. S4 A). MDA-MB-231 cells stably expressing MT1-MMPmCh were double labeled for JIP4 and KIF5B or p150^{Glued}. As expected for motors having pleiotropic associations with various cell organelles, KIF5B and p150^{Glued} showed a cytoplasmic dotty distribution with some association with the cytosolic face of MT1-MMPmCh–containing endosomes decorated by JIP4 puncta (Fig. 3, A and B). Some colocalization was visible between JIP4 and p150^{Glued} (Fig. 3 B, arrows), which was confirmed by in situ proximity ligation assay (PLA; Fig. 3, E and F). PLA signal was strongly reduced upon JIP3/JIP4 knockdown, or when JIP4 or p150^{Glued} antibody was omitted (Fig. 3 F). Altogether, these observations indicate a close proximity between JIP4 and p150^{Glued} on MT1-MMP–positive compartments. In addition, several cytoplasmic puncta of KIF3A were detected in association with Rab7- and MT1-MMPmCh–positive LEs (Fig. 3 C). Double labeling for KIF3A and KIF5B showed that both kinesins were associated with the same MT1-MMP–positive endosomes (Fig. 3 D).

KIF5B-YFP and KIF3A-GFP subunits were stably expressed in MDA-MB-231 cells at levels similar to the endogenous subunits (Fig. S4, B and C). The distribution of MT1-MMPmCh–positive endosomes was more dispersed and peripheral in cells expressing KIF5B-YFP or KIF3A-GFP as compared with control cells expressing YFP (Fig. S4, D and E). Color coding of vesicle movement showed that MT1-MMP endosomes retained both anterograde and retrograde motility (Fig. S4 D, bottom panels). To quantitatively assess differences in motility of MT1-MMPmCh–positive LEs in cells stably expressing KIF5B or KIF3A as compared with control YFP-expressing cells in an unbiased manner, we calculated a displacement index for each cell population (Materials and methods section TIRF microscopy and live cell spinning disk confocal microcopy; Quintero et al., 2009). The displacement index increased ~2.3-fold in cells stably expressing KIF5B or KIF3A as compared with control YFP-expressing cells (Fig. S4 F). In contrast, silencing of KIF5B or KIF3A in MDA-MB-231 cells led to an approximately twofold reduction of overall endosome motility (Fig. S4 G). Altogether, these results indicate that MT1-MMP–positive endosome motility relies on the association and activity of kinesin-1 and -2 and confirm the role of p150^{Glued} dynactin subunit in minus end–directed movement of MT1-MMP–positive LEs in breast cancer cells.

JIP3/JIP4 regulate motor association on MT1-MMP endosomes

Given ARF6 and JIP3/JIP4's roles in MT1-MMP endosome positioning and interaction with kinesin-1 and the dynein–dynactin complex, we investigated the potential implication of ARF6 and JIPs on endosomal association of KIF5B, KIF3A, and p150^{Glued} using two independent approaches. First, Arf6 or JIP3/JIP4 was silenced, and after fixation and IF staining for motor proteins, MT1-MMPmCh–positive compartments were segmented from deconvoluted microscopy images, and the number of puncta of motor proteins associated with each segmented MT1-MMP–positive vesicle was scored (Fig. 3, G and H). Using this approach, we found that JIP3/JIP4 silencing correlated with a 50–60% decrease of KIF5B and p150^{Glued} association with MT1-MMP–positive endosomes, whereas KIF3A association was not affected (Fig. 3, G and H). The effect of ARF6 knockdown was more difficult to analyze, as loss of ARF6 function led to clustering and various extent of MT1-MMP endosome collapse in the cell center (Fig. 2 F). Consequently, motor association values were highly variable for all three motor proteins and increased nonsignificantly, probably as a consequence of endosome enlargement (Fig. 3, G and H).

In addition, association of motor proteins with MT1-MMP cargo was analyzed by coimmunoprecipitation experiments. KIF5B and KIF3A coimmunoprecipitated with MT1-MMP expressed at the endogenous level in MDA-MB-231 cells (Fig. 3 I). In addition, overexpressed MT1-MMPmCh coimmunoprecipitated with GFP-tagged KIF5B or KIF3A (Fig. 3 J). In reciprocal experiments, endogenous KIF5B, p150^{Glued}, or KIF3A coimmunoprecipitated with overexpressed MT1-MMP-mCh in control siNT-treated cells (Fig. 3, K and L). Silencing of JIP3/JIP4 significantly decreased MT1-MMP association with KIF5B and p150^{Glued} proteins, whereas it had no effect on MT1-MMP/KIF3A interaction (Fig. 3, K and L). Noticeably, knockdown of ARF6 did not interfere with the association of MT1-MMP with KIF5B, p150^{Glued}, or KIF3A (Fig. 3, K and L). Thus, our data are consistent with JIP3/JIP4 controlling the transport and dynamics of MT1-MMP storage endosomes through the association of KIF5B/kinesin-1 and dynactin complex with MT1-MMP endosomes, whereas it has no effect on KIF3A/kinesin-2 recruitment.

Finally, we investigated whether KIF3A/kinesin-2 may be responsible for the peripheral distribution of MT1-MMP endosomes observed in cells silenced or inhibited for JIP3/JIP4 (Fig. 2, E and F) as a consequence of kinesin-1 and dynactin loss (Fig. 3, G, H, K, and L). Triple silencing of JIP3/JIP4 and KIF3A changed the distribution of MT1-MMP–positive endosomes, which appeared as clusters scattered in the cytoplasm (Fig. 4, A–C, yellow curve), different from their peripheral distribution in JIP3/JIP4 double-depleted cells (Fig. 4 C, green

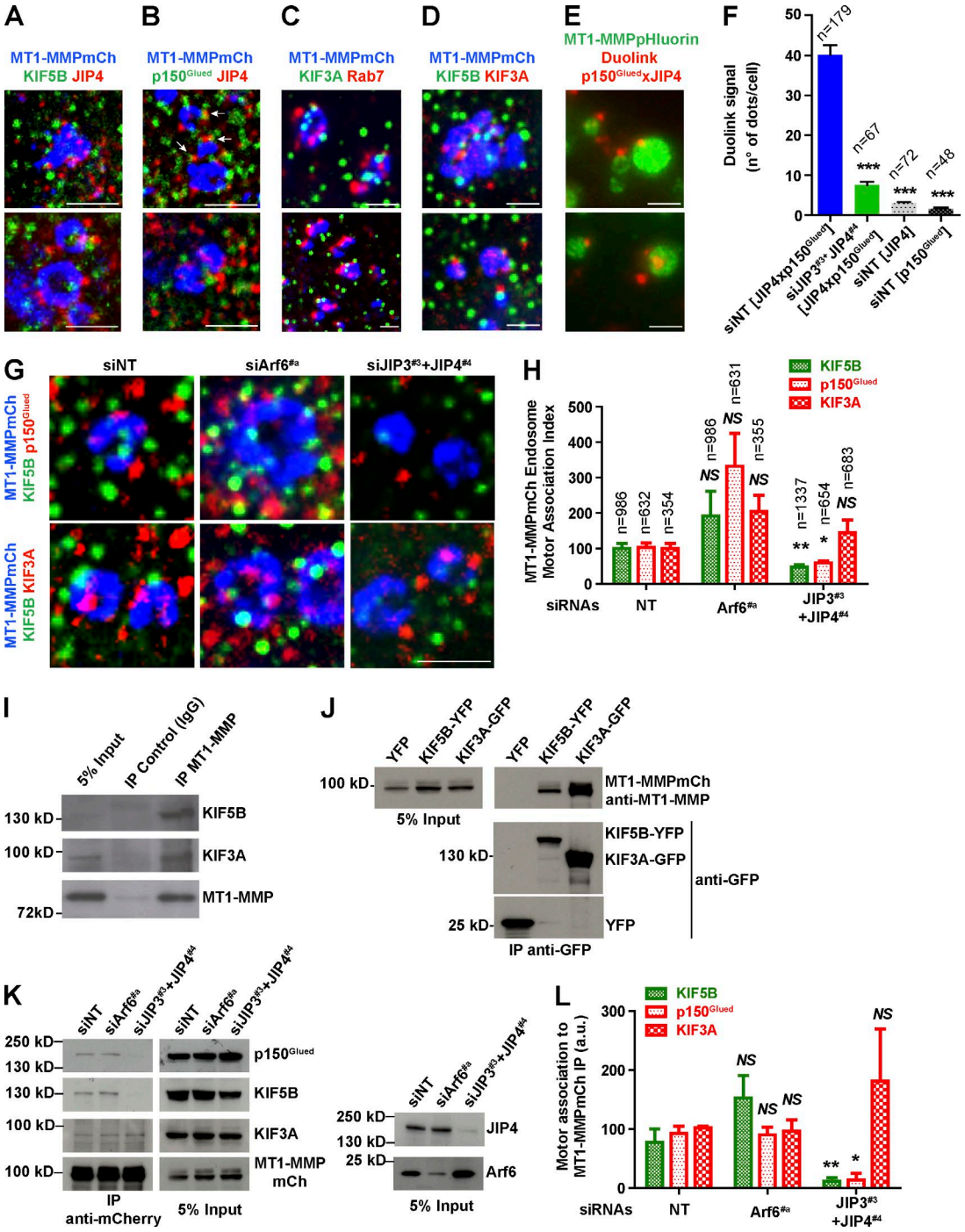

Figure 3. **JIP3/JIP4 regulate KIF5B and p150Glued but not KIF3A association to MT1-MMP endosomes.** (A–D) Association of indicated motor proteins (green and red) with MT1-MMPmCh–positive endosomes. Arrows in B point to JIP4 and p150Glued colocalization. (E) MDA-MB-231 cells expressing MT1-MMP-pHluorin analyzed by in situ PLA (red) with p150Glued and JIP4 antibodies. Bars, 2 µm. (F) PLA signal in siRNA-treated cells using the indicated antibodies (in brackets). Values are mean number of PLA dots/cell ± SEM. *n*, number of cells analyzed for each cell population. (G) MDA-MB-231 cells expressing MT1-MMPmCh treated with the indicated siRNAs and stained for KIF5B and p150Glued (top) or KIF5B and KIF3A (bottom). Bar, 2 µm. (H) Motor protein association (KIF5B, p150Glued, or KIF3A) with MT1-MMP–positive compartments compared with association in siNT-treated control cells (see Materials and methods section 3D deconvolution microscopy). *n*, number of endosomes analyzed for each cell population. (I) Detection of KIF5B and KIF3A endogenous proteins in anti–MT1-MMP immunoprecipitates (IPs) from MDA-MB-231 cells. (J) Detection of MT1-MMPmCh in anti-GFP IPs of YFP, KIF5B-YFP, or KIF3A-GFP. (K) Detection of KIF5B, p150Glued, and KIF3A motor proteins in MT1-MMPmCh IPs from MDA-MB-231 cells transfected with the indicated siRNAs. (L) Quantification of motor association from immunoblotting analysis as in I. Levels in siNT control cells were set to 100. *, $P < 0.05$; **, $P < 0.01$; ***, $P < 0.001$ (as compared with siNT-treated cells).

curve) or the perinuclear one in KIF3A single-depleted cells (Fig. 4 C, purple curve). Analysis of vesicle movement revealed that MT1-MMP endosome clusters in JIP3/JIP4-KIF3A triple-depleted cells were mostly immobile, similar to the situation observed in nocodazole-treated cells and consistent with motorless MT1-MMP endosomes (Fig. 4, D–F; and Video 2).

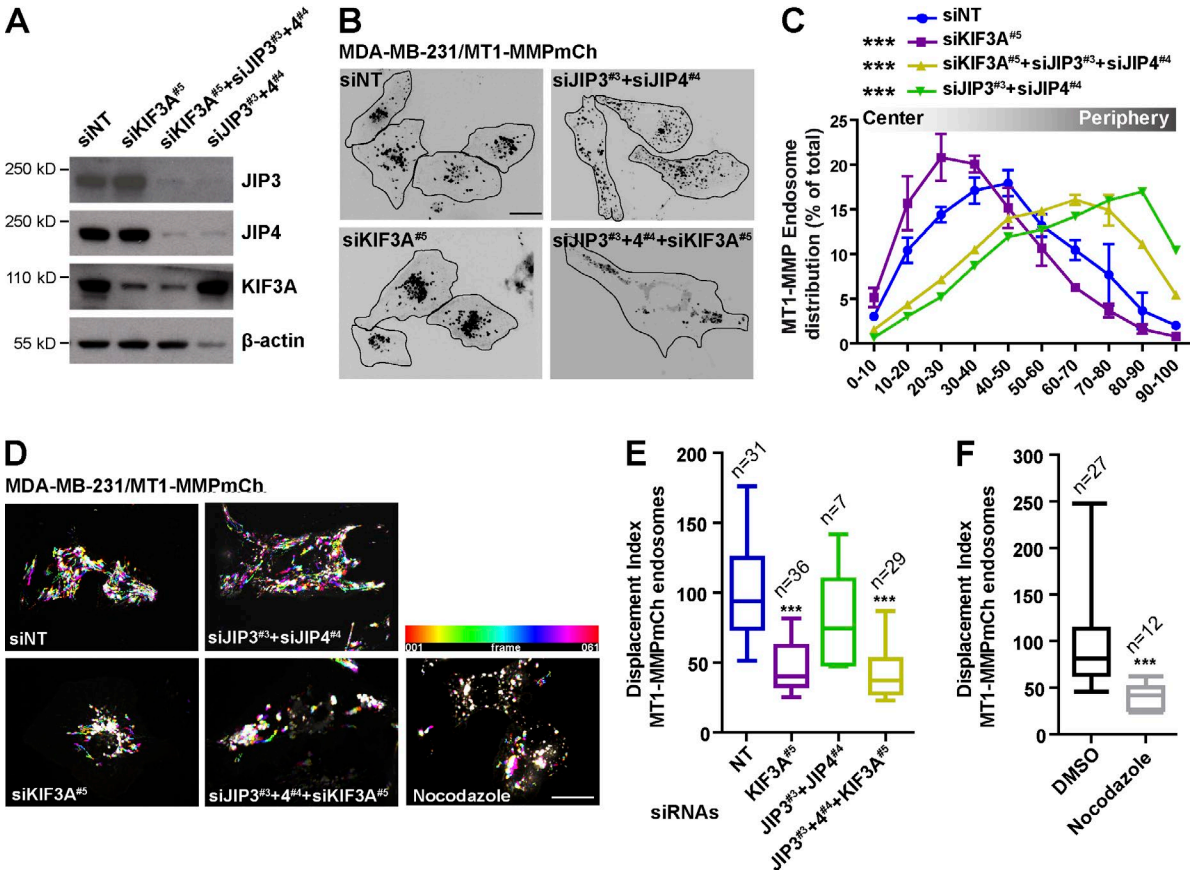

Figure 4. **KIF3A mediates peripheral distribution of the MT1-MMP endosome in JIP3/JIP4-depleted cells.** (A) Silencing of KIF3A and JIP3/4 in MT1-MMP-mCh–expressing MDA-MB-231 cells. β-Actin was used as a loading control. (B) Inverted still images from time-lapse sequences of MDA-MB-231 cells expressing MT1-MMPmCh endosomes treated with the indicated siRNAs (see Video 2). Bar, 5 µm. (C) Mean percentage distribution of MT1-MMPmCh–positive endosomes according to their cell center-to-cell periphery position ± SEM. ***, $P < 0.001$ (compared with siNT-treated cells). (D) Color-coded time projections of 61 consecutive time frames from time-lapse sequences of MDA-MB-231 cells expressing MT1-MMPmCh (acquired with 3-s intervals). Bar, 5 µm. (E and F) Displacement index of MT1-MMP–positive endosomes in indicated cell populations. ***, $P < 0.001$ (compared with siNT-treated cells in E or DMSO-treated cells in F). *n*, number of scored cells.

Thus, kinesin-2 redistributes MT1-MMP endosomes to the cell periphery in JIP3/JIP4-deficient cells.

ARF6, JIP3/JIP4, and p150^{Glued} are required for KIF5B-mediated MT1-MMP endosome tubulogenesis

Functional consequences of kinesin-mediated movement of MT1-MMP–containing endosomes on the invasive potential of breast tumor cells were assessed. Silencing of KIF3A or KIF5B with independent siRNA pairs (Fig. 5, A–C) resulted in a strong reduction in MDA-MB-231 cells' ability to degrade FITC-gelatin and to invade a 3D type I collagen matrix in a circular invasion assay, similar to MT1-MMP knockdown (Fig. 5, D and E). Similar effects were observed upon silencing of KIF5B or KIF3A in MCF10DCIS.com cells (Fig. 5, F and G). In addition, silencing of KIF3A or KIF5B decreased pericellular type I collagen proteolysis in association with a reduction of MT1-MMP-pHluorin exocytosis (Fig. 5, H and I).

We then focused our analysis on KIF5B, whose association with MT1-MMP endosomes is regulated by JIP3/JIP4. ARF6 silencing shifted the scattered distribution of MT1-MMP–positive compartments in KIF5B-overexpressing cells to the perinuclear region, confirming that loss of ARF6 function strongly promoted minus end dynactin–dynein complex-dependent movement dominantly over KIF5B overexpression (Fig. 6, A and B, compare brown and blue curves). As already observed in parental MDA-MB-231 cells (Fig. 2, E and F), knockdown of JIP3/JIP4 triggered a peripheral distribution of MT1-MMP endosomes (Fig. 6, A and B, green and blue curves) probably dependent on KIF3A (Fig. 4). Similarly, p150^{Glued} knockdown resulted in a shift of endosome distribution toward the cell periphery, likely as a consequence of loss of kinesin-antagonizing activity of the dynactin–dynein complex (Fig. 6, A and B, pink and blue curves).

Next, we investigated the matrix degradative capacity of the different KIF5B-overexpressing cell populations. Correlating with increased dynamics and peripheral distribution of MT1-MMP–positive endosomes (Fig. S4), overexpression of KIF5B resulted in a dramatic 3.5-fold up-regulation of FITC-gelatin degradation capacity (Fig. 6 C). As in parental MDA-MB-231 cells (Fig. 1 A), loss of ARF6 function causing perinuclear accumulation of MT1-MMP endosomes abolished the matrix degradation–promoting effect of KIF5B overexpression (Fig. 6 C and Fig. S5, A and C). More surprising was the observation that JIP3/JIP4 loss of function also interfered with gelatin degradation by KIF5B-overexpressing cells despite a pronounced peripheral distribution of MT1-MMP–positive endosomes (Fig. 6 C and Fig. S5, A and C). Similarly, p150^{Glued}

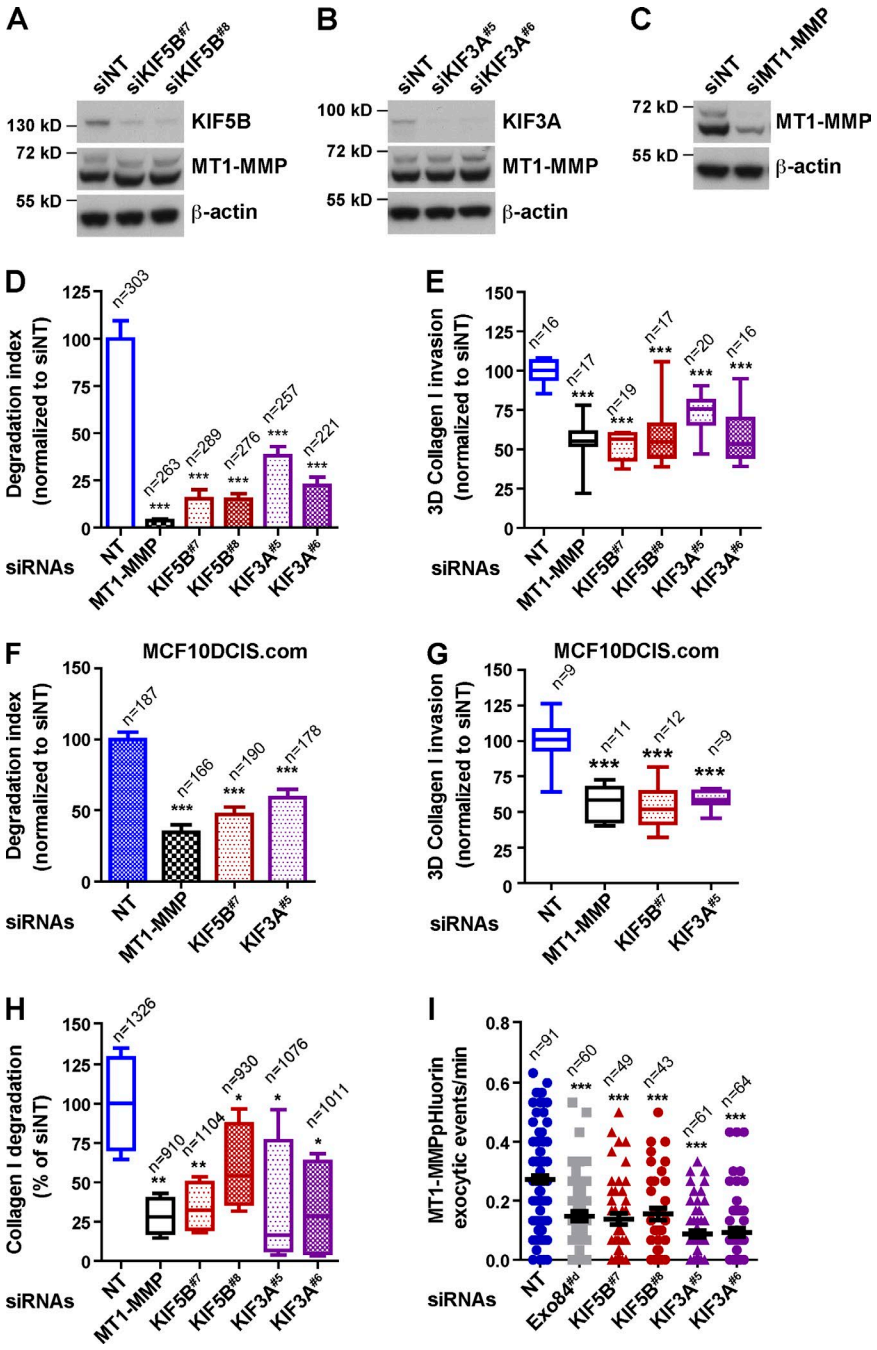

Figure 5. **KIF5B and KIF3A are required for pericellular matrix remodeling and MT1-MMP exocytosis.** (A–C) Silencing of KIF5B, KIF3A, and MT1-MMP in MDA-MB-231 cells. β-Actin was used as a loading control. (D) FITC-gelatin degradation. *n*, number of cells scored for each MDA-MB-231 cell population treated with the indicated siRNA. (E) Mean invasion area of MDA-MB-231 cells using the circular invasion assay. Values represent mean invasion index ± SEM from three independent experiments normalized to invasion index of siNT-treated cells set to 100. *n*, number of 96 wells analyzed for each cell population. (F) FITC-gelatin degradation by MCF10DICIS.com cells treated with indicated siRNAs as in D. (G) Invasion of MCF10DICIS.com cells as in E. (H) Collagenolysis by MDA-MB-231 cells treated with indicated siRNAs. Values are mean normalized degradation index ± SEM. *n*, number of cells analyzed for each cell population. (I) MDA-MB-231 cells expressing MT1-MMPpHluorin silenced for the indicated proteins were seeded on type I collagen fibers and imaged over a 30-min time period. Frequency of MT1-MMPpHluorin exocytic events was quantified (events/cell/minute). *n*, number of cells analyzed for each cell population. *, $P < 0.05$; ***, $P < 0.001$ (as compared with siNT-treated cells).

knockdown affected matrix degradation by KIF5B-overexpressing cells (Fig. 6 C and Fig. S5, B and C). Thus, like in MDA-MB-231 parental cells, loss of ARF6 or JIP3/JIP4 function, although having opposite effects on MT1-MMP endosome distribution, resulted in similar impairment of the pericellular matrix degradative activity of MDA-MB-231, which could not be compensated for by KIF5B overexpression and/or endogenous KIF3A activity.

Surface delivery of MT1-MMP involves the formation of tubular connections between storage endosomes and the plasma membrane in association with ECM fibers (Steffen et al., 2008; Monteiro et al., 2013). Close inspection of time-lapse videos of MT1-MMPmCh endosomes in cells overexpressing KIF5B revealed highly dynamic tubular structures forming from MT1-MMP–positive vesicular compartments in the vicinity of the ventral plasma membrane in contact with the matrix (Fig. 6 D, siNT; and Video 3). Time-lapse total internal reflection fluorescence (TIRF) microscope analysis confirmed that tubulogenesis from MT1-MMP endosomes took place in association with the plasma membrane (Fig. 6 E). Knockdown of JIP3/JIP4 diminished tubulogenesis of the MT1-MMP endosome in the vicinity of the ventral cell surface by twofold (Fig. 6, D and F; and Video 3). This finding suggests that KIF3A activity, which is responsible for peripheral accumulation of MT1-MMP–positive compartments at the microtubule plus end in JIP3/JIP4-depleted cells (Fig. 4), does not support tubulogenesis. Along this line, KIF3A silencing did not significantly affect tubulogenesis (Fig. 6, D and F). In addition, silencing of $p150^{Glued}$ inhibited endosomal tubule formation, indicating that dynactin function is also required for tubulogenesis from MT1-MMP–pos-

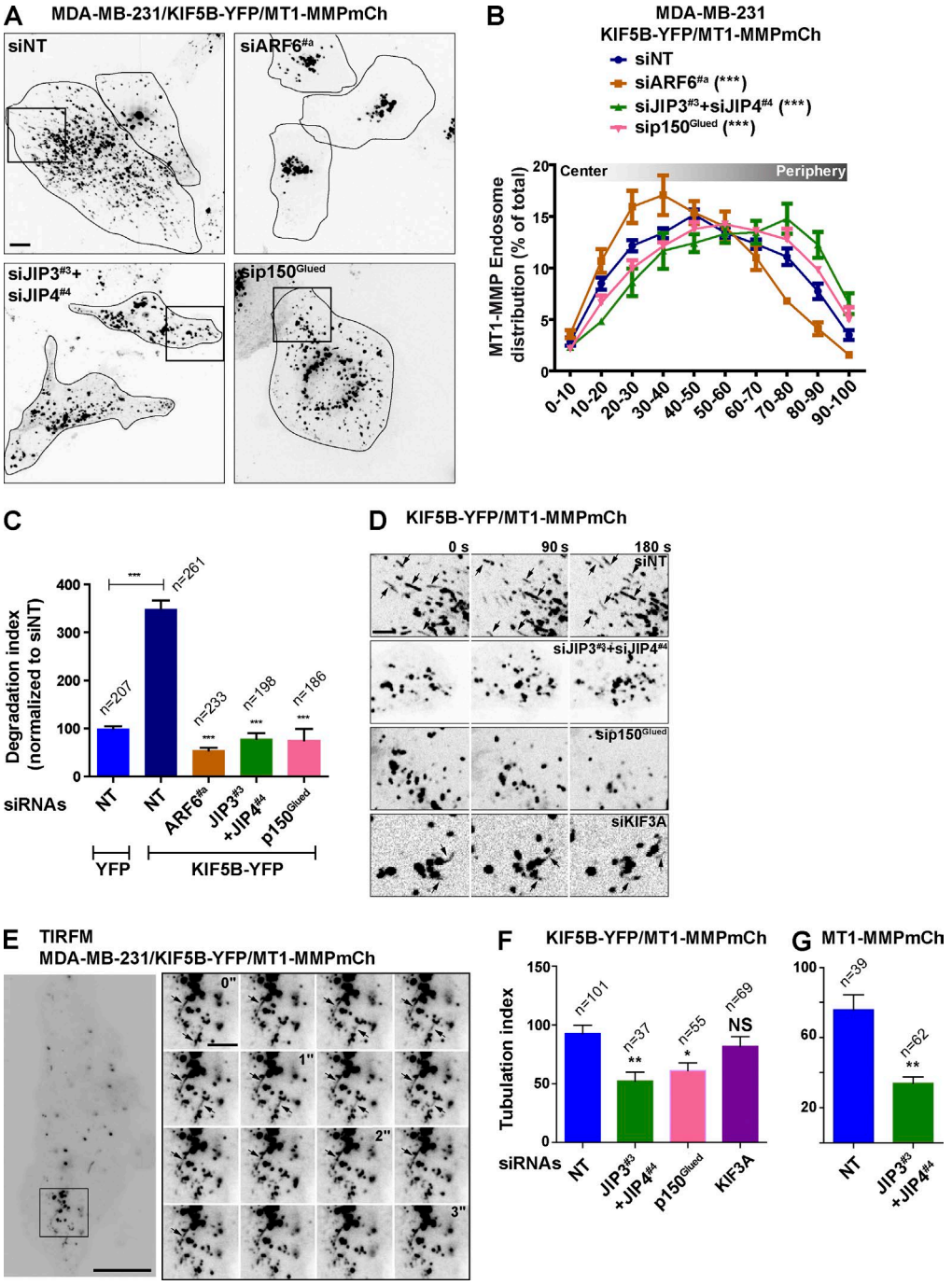

Figure 6. **Stimulation of matrix degradation by KIF5B correlates with increased ARF6-, JIP3/4-, and p150Glued-dependent endosome tubulogenesis.** (A) Inverted still images from time-lapse sequences of MDA-MB-231 cells expressing KIF5B-YFP and MT1-MMPmCh treated with the indicated siRNAs (see Video 3). Bar, 10 µm. (B) Mean percentage distribution of MT1-MMPmCh–positive endosomes according to their cell center-to-cell periphery position ± SEM. (C) FITC-gelatin degradation by MDA-MB-231 cells overexpressing MT1-MMPmCh together with YFP or KIF5B-YFP. *n*, number of cells scored for each MDA-MB-231 cell population treated with the indicated siRNAs. (B and C) ***, $P < 0.001$ (as compared with siNT-treated cells). (D) High-magnification galleries of peripheral cell regions (boxed in A). Arrows point to tubulated MT1-MMP endosomes. Bar, 5 µm. (E) TIRF microscopy images of MDA-MB-231 cells expressing MT1-MMPmCh and KIF5B-YFP plated on gelatin. Gallery shows images with 0.2-s intervals corresponding to the boxed region. Arrows point to membrane tubulation events. Bars: 5 µm; (gallery) 2 µm. (F and G) Number of tubulated MT1-MMPmCh endosomes per frame normalized for the surface area. Mean ± SEM. *n*, number of peripheral cell regions scored for each cell population. *, $P < 0.05$; **, $P < 0.01$ (as compared with siNT condition).

itive compartments (Fig. 6, D and F; and Video 3). Notably, tubule formation was not detected from perinuclear clustered MT1-MMP endosomes in ARF6-depleted cells (not depicted). Tubulogenesis was also visible in MDA-MB-231 cells with an endogenous kinesin-1 level, although to a lower extent (not depicted; Steffen et al., 2008; Monteiro et al., 2013), and was diminished by twofold upon JIP3/JIP4 knockdown (Fig. 6 G; Steffen et al., 2008; Monteiro et al., 2013). Thus, we conclude that impaired MT1-MMP exocytosis and pericellular matrix remodeling upon knockdown of the ARF6, JIP3/JIP4, or p150Glued

dynactin complex subunit correlate with the decreased tubulogenesis capacity of MT1-MMP–positive endosomes in association with subplasmalemma microtubules.

WASH is required for JIP4 association and function on MT1-MMP endosomes

So far, our data pointed to an essential role of tubulogenesis of peripheral MT1-MMP storage endosomes for MT1-MMP targeting to the plasma membrane based on a mechanism requiring ARF6 and JIP3/JIP4 controlling KIF5B/kinesin-1 and $p150^{Glued}$/dynactin proteins. We reported earlier that formation of tubular connections between MT1-MMP–containing LEs and the plasma membrane and MT1-MMP exocytosis required the WASH complex (Monteiro et al., 2013). The punctate staining of JIP4 (Fig. 2 A) was reminiscent of WASH and Arp2/3 complex/cortactin/F-actin distribution on MT1-MMP endosomes (Monteiro et al., 2013; Rossé et al., 2014). Thus, we compared the localization of JIP4 and cortactin in MDA-MB-231 cells and found a close apposition of puncta of the two proteins on the cytosolic face of MT1-MMPmCh–positive endosomes (Fig. 7 A). Moreover, WASH knockdown led to a strong reduction of cortactin puncta on MT1-MMP endosomes paralleled by an even stronger loss of JIP4 (Fig. 7, A and B; and Fig. S5 D). Thus, JIP4 association to MT1-MMP endosomes requires WASH. Similar to the effects of JIP3/JIP4 depletion, silencing of WASH in MDA-MB-231 cells overexpressing KIF5B decreased tubulogenesis of peripherally located MT1-MMP endosomes and strongly inhibited the gelatin degradation capacity of the cells (Fig. 7, C–E; and Fig. S5 E). Altogether, our data suggest that ARF6 and JIP3/JIP4 control a tug-of-war mechanism of kinesin-1 and dynactin–dynein involved in endosome tubulogenesis, possibly in conjunction with the WASH- and F-actin–based endosome membrane deformation required for MT1-MMP exocytosis in breast cancer cells (see Discussion and model in Fig. 7, F and G).

ARF6, MT1-MMP, and KIF5B up-regulation in TNBCs

Data on ARF6 expression in breast cancers have been missing because of a lack of suitable ARF6 antibodies for IHC of clinical specimens. One monoclonal anti-ARF6 antibody was selected and its specificity validated based on the loss of IHC signal on a section of multicellular spheroids of MCF10DCIS.com cells knocked down for ARF6 expression (not depicted). Changes in ARF6 levels in breast carcinoma cells and association with breast cancer markers were investigated by IHC analysis of a tissue microarray (TMA) of invasive ductal carcinomas (IDCs; characteristics of 496 patients summarized in Table S1; Lodillinsky et al., 2015). ARF6 staining was diffuse and cytosolic in luminal epithelial cells from peritumoral breast epithelial tissues (Fig. 8 A and see Fig. 10 B) and was also detected in myoepithelial and stromal cells, including fibroblasts and immune cells (not depicted). Based on analysis of 426 IDCs available for scoring and using an H-score method (intensity score × percentage of positive cells), levels of cytosolic ARF6 were significantly higher in carcinoma cells as compared with adjacent epithelial cells in peritumoral tissues, whereas there was no significant difference between in situ and invasive components of IDCs (Fig. 8, A and B). Strikingly, ARF6 was present at cell–cell contacts in a subset of tumors (107/426, 25.1%; Fig. 8 A and see Fig. 10 B). Membranous ARF6 staining was restricted to carcinoma cells and never detected in normal breast epithelial cells in peritumoral tissues, and it was significantly higher in invasive versus in situ components of IDCs, particularly in TNBCs (Fig. 8 C and Fig. 9 F).

These data indicate that ARF6 is up-regulated during breast tumor progression and accumulates at the plasma membrane of carcinoma cells in IDCs, possibly as a result of hyperactivation (Morishige et al., 2008). We previously reported that MT1-MMP levels increased at the surface of carcinoma cells in TNBCs based on IHC analysis of the TMA of human IDCs (Lodillinsky et al., 2015). A similar analysis was performed for KIF3A and KIF5B to test the hypothesis that ARF6 may cooperate with motor proteins during MT1-MMP–dependent cell invasion in invasive breast cancers. The semiquantitative H-score method was used for the four markers based on specific staining patterns (i.e., membranous ARF6 and MT1-MMP and total KIF3A and KIF5B; Fig. 9, A–D; and Fig. 10, A–D). For all four markers, levels were significantly higher in cancer cells as compared with mammary epithelial cells in peritumoral tissues (Fig. 9 E). Based on 311 IDCs available for scoring, levels of membranous ARF6, surface MT1-MMP, and KIF5B were positively correlated (Table S2 and Table S3) and significantly increased in high-grade (grade 3) tumors; all three markers were higher in estrogen receptor (ER)– and progesterone receptor (PR)–negative tumors, particularly in TNBCs (Fig. 9, F and G). In contrast, KIF3A levels negatively correlated with ARF6 and MT1-MMP expression (Table S2 and Table S3) and were higher in lower grades and in ER- and PR-positive (luminal) tumors (Fig. 9, F and G). A hierarchical clustering algorithm was applied for the analysis of H scores. ARF6, MT1-MMP, and KIF5B co-clustered in their staining patterns, whereas KIF3A segregated away (Fig. 10 E). Hierarchical clustering analysis showed that the 311 IDCs segregated into two main branches; one of the branches comprised a subgroup of 30 IDCs with strong staining for ARF6, MT1-MMP, and KIF5B markers and low KIF3A levels corresponding mostly to grade 3 (27/30) TNBCs (20/30; Fig. 10 E). Collectively, these data suggest an interplay of ARF6, KIF5B, and MT1-MMP in aggressive high-grade TNBCs.

Discussion

ARF6 was shown early on to localize to invadopodia, specialized matrix degradative structures of tumor cells, and to be required for invadopodial activity (Hashimoto et al., 2004; Tague et al., 2004). Pioneering work identified an ARF6 pathway in which ARF6 activated by the guanine nucleotide exchange factor GEP100 at the plasma membrane is pivotal for invasion and metastasis of breast tumor–derived cell lines (Onodera et al., 2005, 2012; Hashimoto et al., 2006; Morishige et al., 2008). Here, we found that ARF6, MT1-MMP, and KIF5B kinesin-1 heavy chain subunit are abnormally overexpressed in high-grade TNBCs. To our knowledge, this is the first study reporting on dysregulation of ARF6 protein levels and its correlation with MT1-MMP in breast tumor specimens. Up-regulation of ARF6, MT1-MMP, and KIF5B in TNBCs is pathologically highly relevant given the correlation between MT1-MMP levels and tumor progression and increased metastatic potential in this subgroup of highly aggressive breast cancers (Perentes et al., 2011; Lodillinsky et al., 2015).

MT1-MMP is targeted to endosomal compartments after endocytosis from the cell surface and is then recycled mainly

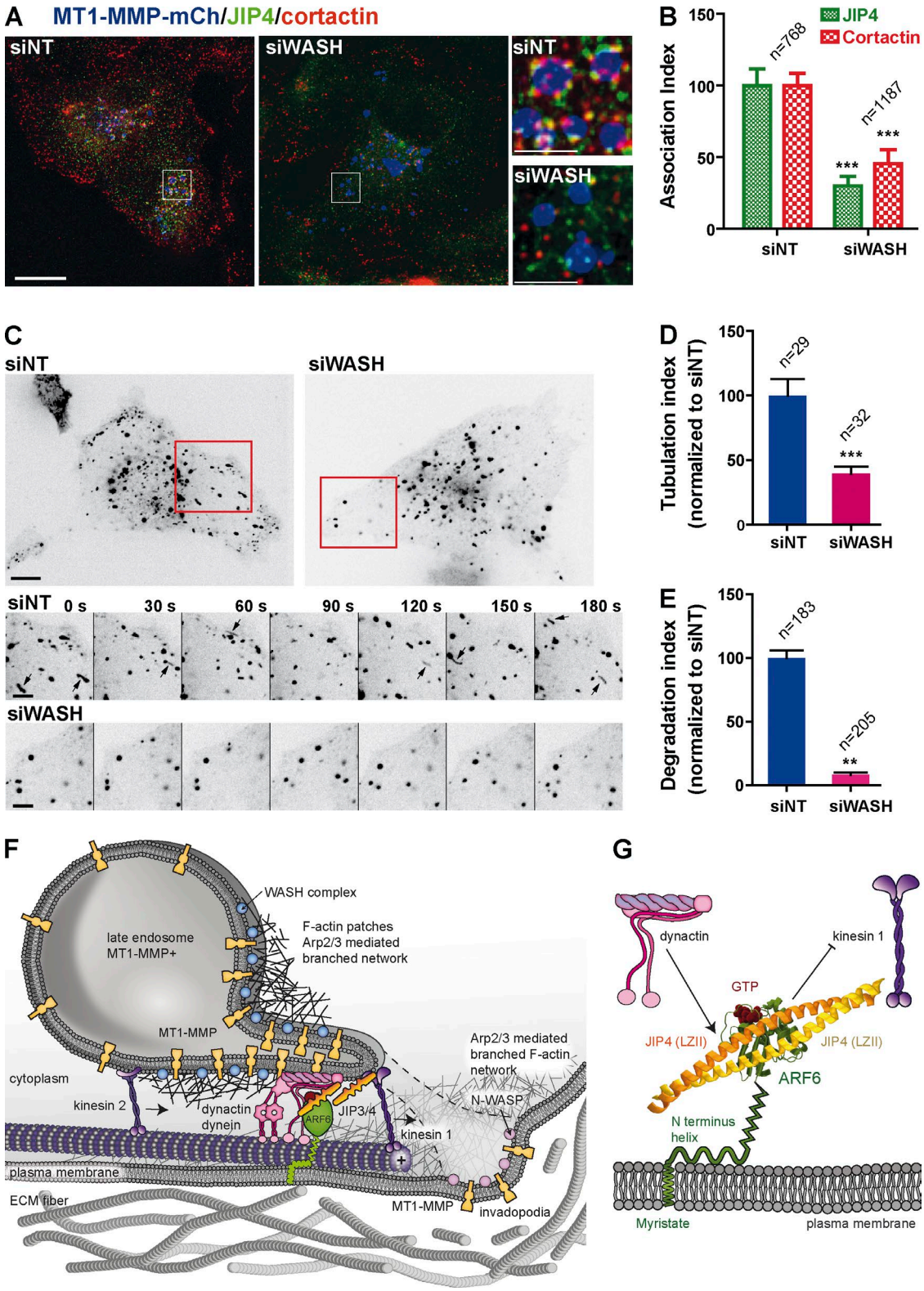

Figure 7. **JIP4 recruitment on MT1-MMP–positive endosomes depends on WASH.** (A) JIP4 and cortactin staining of MDA-MB-231 cells expressing MT1-MMPmCh treated with the indicated siRNAs. Bars: 5 µm; (insets) 1.25 µm. (B) JIP4 and cortactin association with MT1-MMPmCh–positive endosomes as in Fig. 3 H. ***, $P < 0.001$ (as compared with siNT-treated cells in which association was set to 100). (C) Inverted still images from time-lapse sequences of MDA-MB-231 cells expressing KIF5B-YFP and MT1-MMPmCh treated with the indicated siRNAs. Bar, 10 µm. Galleries show images with 30-s intervals corresponding to the boxed regions. Arrows point to tubulated endosomes. Bar, 5 µm. (D) Quantification of tubulation from time-lapse sequences as in C. All values are mean ± SEM. *n*, number of cell regions scored for each cell population. ***, $P < 0.001$ (as compared with siNT-treated cells). (E) FITC-gelatin degradation by MDA-MB-231 cells overexpressing MT1-MMPmCh and KIF5B-YFP treated with indicated siRNAs. *n*, number of cells scored for each cell population. **, $P < 0.01$ (compared with siNT-treated cells). (F) Scheme depicting ARF6 and JIP3/JIP4-mediated regulation of a kinesin-1 and dynactin–dynein tug of war leading to MT1-MMP endosome tubulation and surface delivery of MT1-MMP (see Discussion). (G) Model of trans-interaction

from late endocytic storage compartments back to the surface of invasive TNBC cells (Steffen et al., 2008; Williams and Coppolino, 2011; Yu et al., 2012; Hoshino et al., 2013; Monteiro et al., 2013). Exocytosis of MT1-MMP occurs at invadopodia forming at matrix contact sites where MT1-MMP is essential for remodeling specific pericellular ECM substrates required for transmigration of cancer cells through the basement membrane, locoregional invasion, and tumor growth and metastasis (Hotary et al., 2003, 2006; Artym et al., 2006; Hu et al., 2008; Perentes et al., 2011; Hoshino et al., 2013; Monteiro et al., 2013; Lodillinsky et al., 2015). As ARF6 activation (GTP binding) involves guanine exchange factors associated with the plasma membrane (D'Souza-Schorey and Chavrier, 2006; Donaldson and Jackson, 2011), up-regulation of membranous ARF6 in high-grade TNBCs suggests that it is the active form of ARF6 that may accumulate at the plasma membrane in this subset of highly invasive breast tumors coincident with elevated MT1-MMP surface levels.

These data reveal the importance of ARF6 in orchestrating cooperative mechanisms to promote MT1-MMP exocytosis from late endosomal compartments and to drive the invasive potential of TNBC cells. Our findings are integrated in a model shown in Fig. 7 (F and G). MT1-MMP–positive endosomes undergo bidirectional movements along microtubules through opposing activities of dynactin–dynein and kinesin-1 and kinesin-2. Experimentally, a normal balance of opposing motors can be perturbed by dynactin, KIFB5, or KIF3A gene silencing (or overexpression) with a resulting bias of MT1-MMP endosome movement toward the plus or minus end. Recruitment of KIF5B kinesin-1 and $p150^{Glued}$ dynactin subunits on MT1-MMP–containing vesicles depends on JIP3 and JIP4, in contrast to the association of KIF3A kinesin-2 subunit that is JIP independent. JIP4 associates as patches with the cytosolic face of the limiting membrane of MT1-MMP–positive endosomes (localization data for JIP3 are not available). JIP4 patches are closely apposed to and require WASH-positive puncta for endosomal association. Through kinesins, MT1-MMP–positive endosomes reach the cell periphery and the plasma membrane in contact with the ECM. A high level of activated GTP-ARF6 at the plasma membrane interacts in trans with JIP3/JIP4 on the endosomal membrane. This scenario is compatible with the crystal structure of GTP-ARF6 bound to the second coiled-coil (LZII) domain of JIP4 (Fig. 7 G; Isabet et al., 2009).

Based on our previous biochemical evidence, binding of GTP-ARF6 to the LZII domain of JIP3/JIP4 dimers occurs preferentially with JIP3/JIP4 bound to dynactin ($p150^{Glued}$). In contrast, JIP3/JIP4 association with the tetratricopeptide repeat domain of kinesin-1 light chain may preclude binding of ARF6 to JIP3/JIP4 (Montagnac et al., 2009). We postulate that trans-interaction of GTP-ARF6 with the JIP3/JIP4-dynactin complex keeps dynein on the leash in a state in which dynein associated with MT1-MMP endosome remains firmly anchored on the microtubule, a situation analogous to the effect of LIS1 acting as a clutch that suppresses dynein movement (McKenney et al., 2010; Huang et al., 2012). In support of this assumption, we observed that the loss of ARF6 function correlated with strong dynactin–dynein-dependent perinuclear positioning of MT1-MMP–positive compartments, whereby increased dynein processivity is possibly caused by JIP3/JIP4 interacting with dynactin, as shown recently for cargo adaptors such as Bicaudal or FIP3 (King and Schroer, 2000; McKenney et al., 2014; Tripathy et al., 2014). Several studies have reported how kinesins and dynein–dynactin localized on the same cargo can mechanically compete in a tug-of-war mechanism (Hancock, 2014). A recent study in particular showed in a quantitative model how endosomes become elongated as a result of the two types of motors pulling in opposite directions (Soppina et al., 2009). Thus, we postulate that kinesin-1, possibly pushed by JIP3/JIP4 (Sun et al., 2011), pulls on the membrane of immobilized MT1-MMP–positive endosomes in a tug a war with stalled dynein–dynactin, leading to tube elongation (Fig. 7 F).

We previously reported that MT1-MMP exocytosis at invadopodia involves the formation of tubular membrane connections between MT1-MMP–containing LEs and the invadopodial plasma membrane (Monteiro et al., 2013). We found that endosomal WASH is required for MT1-MMP exocytosis, possibly by controlling actin-based endosomal membrane deformation required for membrane tubulation (Temkin et al., 2011; Derivery et al., 2012; Gomez et al., 2012). Juxtaposition of JIP3/JIP4 and WASH patches on the endosomal membrane would allow optimal coupling between actin-based membrane deformation and pulling force generation through kinesin-1 for membrane tube generation. Kinesin-2, which is not coordinated with dynactin–dynein through ARF6–JIP3/JIP4, cannot substitute for kinesin-1 for tube generation, clearly indicating nonredundant functions of endosomal kinesin-1 and -2. Then, fusion of the membrane tube with the invadopodial plasma membrane allows transfer of MT1-MMP to the cell surface (Steffen et al., 2008; Yu et al., 2012; Monteiro et al., 2013). In a final step, GTP-hydrolysis on ARF6 to let dynein off the leash would allow clearance of MT1-MMP–positive endosomes from the cell periphery. This mechanism allows MT1-MMP endosomes to dynamically move and switch direction and provides invasive cancer cells with the necessary plasticity to adapt to changing ECM microenvironments. In conclusion, we have delineated the mechanism by which ARF6 through JIP3/JIP4 controls intracellular trafficking and exocytosis of MT1-MMP to promote pericellular matrix remodeling during invasion by TNBCs. Components of the ARF6–JIP3/4 motor axis represent potential important targets in aggressive TNBCs that currently lack targeted therapies.

Materials and methods

DNA constructs and antibodies

Plasmid encoding MT1-MMPmCh has been previously described (Sakurai-Yageta et al., 2008). In brief, human MT1-MMP cDNA obtained from RZPD GmbH was inserted in HindIII and XbaI sites of pcDNA3.1(+) with a geneticin resistance. mCherry (a gift from R.Y. Tsien, University of California, San Diego, La Jolla, CA) was inserted by polymerase chain reaction (PCR) between aa 534 and 535 of MT1-MMP with a GlyGly spacer on both sides of mCherry. Plasmid encoding MT1-MMPpHluorin (Lizárraga et al., 2009) was obtained by

between plasma membrane GTP-ARF6 and endosomal JIP4. ARF6 myristoylated amphipatic N-terminal helix is indicated as a green cylinder lying against the plasma membrane. Only the second coiled coil domain of JIP4 is shown. Binding of GTP-ARF6 to JIP4 dimer is compatible with the dynactin–dynein interaction with JIP4, whereas it prevents kinesin-1 interaction (based on structural and biochemical data; Isabet et al., 2009; Montagnac et al., 2009).

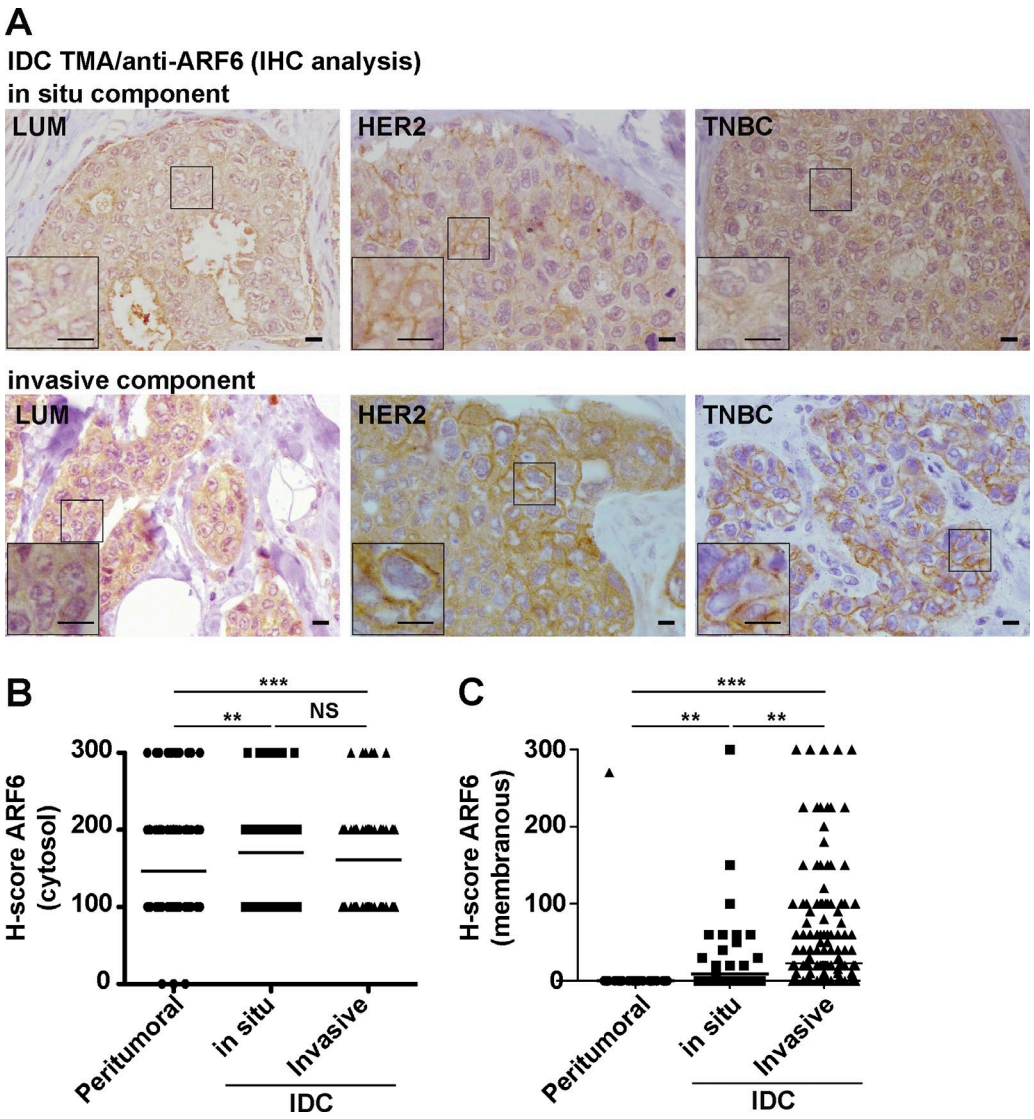

Figure 8. **ARF6 expression increases during breast tumor progression.** (A) ARF6 expression in representative regions of in situ (top) and invasive components (bottom) of IDC of the indicated molecular subtypes stained for ARF6 by IHC. LUM, hormone receptor positive (Luminal A + B); TNBC, hormone receptor negative, HER2 negative; HER2, hormone receptor negative, HER2 positive. Insets are higher magnification of boxed regions. Bars, 10 µm. (B and C) Semiquantitative analysis of cytosolic (B) and membranous ARF6 expression (C) by the H-score method comparing peritumoral breast epithelial tissue (n = 324), in situ (n = 131), and invasive (n = 426) components of IDCs. Comparisons were made with the Kruskal-Wallis test. **, $P < 0.01$; ***, $P < 0.001$.

inserting super ecliptic pHluorin (a gift from T. Galli, Institut Jacques Monod, Paris, France) by PCR between aa 534 and 535 of MT1-MMP with a GlyGly spacer on both sides of pHluorin. MT1-MMP fusion sequences were expressed under control of a cytomegalovirus (CMV) promoter. Plasmids encoding KIF5B-YFP and KIF3A-GFP (gifts from S. Linder, University Medical Center Eppendorf, Hamburg, Germany) have been previously described (Wiesner et al., 2010). The coding sequence of KIF5B was amplified by PCR and inserted between EcoRI and SalI sites of pEYFP-N1 vector (Takara Bio Inc.) under a CMV promoter. The coding sequence of KIF3A was PCR cloned from a human fetal brain library and subcloned between the EcoRI and SalI–XhoI sites of pEGFP-C2 (Takara Bio Inc.) under a CMV promoter. JIP3 LZI domain (aa 1–266) was obtained by PCR amplification from full-length human JIP3 cDNA by using oligos 5′-CAGATGCTCGAGATGATG GAGATCCAGATG-3′ and 5′-CAGATGGAATTCCTGGGTGTGGC GGCCGCCGAG-3′ and subcloned into pEGFP-C3 (Takara Bio Inc.) between XhoI–EcoRI sites (underlined in oligonucleotide sequences; Montagnac et al., 2009). GFP-LZI JIP3$^{L83P/L89P}$ was obtained by PCR site-directed mutagenesis using oligos 5′-CTGGAGCTGCCCC GCGAGGACAACGAGCAGCCCCTCACCCAG-3′ and 5′-CTG GGTGAGGGGCTGCTCGTTGTCCTCGCGGGGCAGCTCCAG-3′ and the plasmid encoding GFP-LZI JIP3 as a template. Leucine residues at positions 83 and 89 were mutagenized into proline using the QuikChange II Site-Directed Mutagenesis Kit (Agilent Technologies). A retroviral plasmid encoding H2B-GFP subcloned in pBabe-puro was provided by F.A. Dick (Addgene plasmid 26790; University of Western Ontario, London, Ontario, Canada; Coschi et al., 2010). A list of antibodies used for these studies is provided in Table S4. Anti-KIF5B and -β1 integrin polyclonal antibodies were gifts from R. Vale (University of California, San Francisco, San Francisco, CA) and C. Albiges Rizo (Institut Albert Bonniot, Grenoble, France), respectively.

Cell culture, transfection, and generation of stable cell lines

Human breast adenocarcinoma MDA-MB-231 cells (HTB-26; ATCC) were maintained in L15 culture medium (Sigma-Aldrich) with 2 mM glutamine (Gibco) and 15% FBS (Gibco) at 37°C in 1% CO_2. To gen-

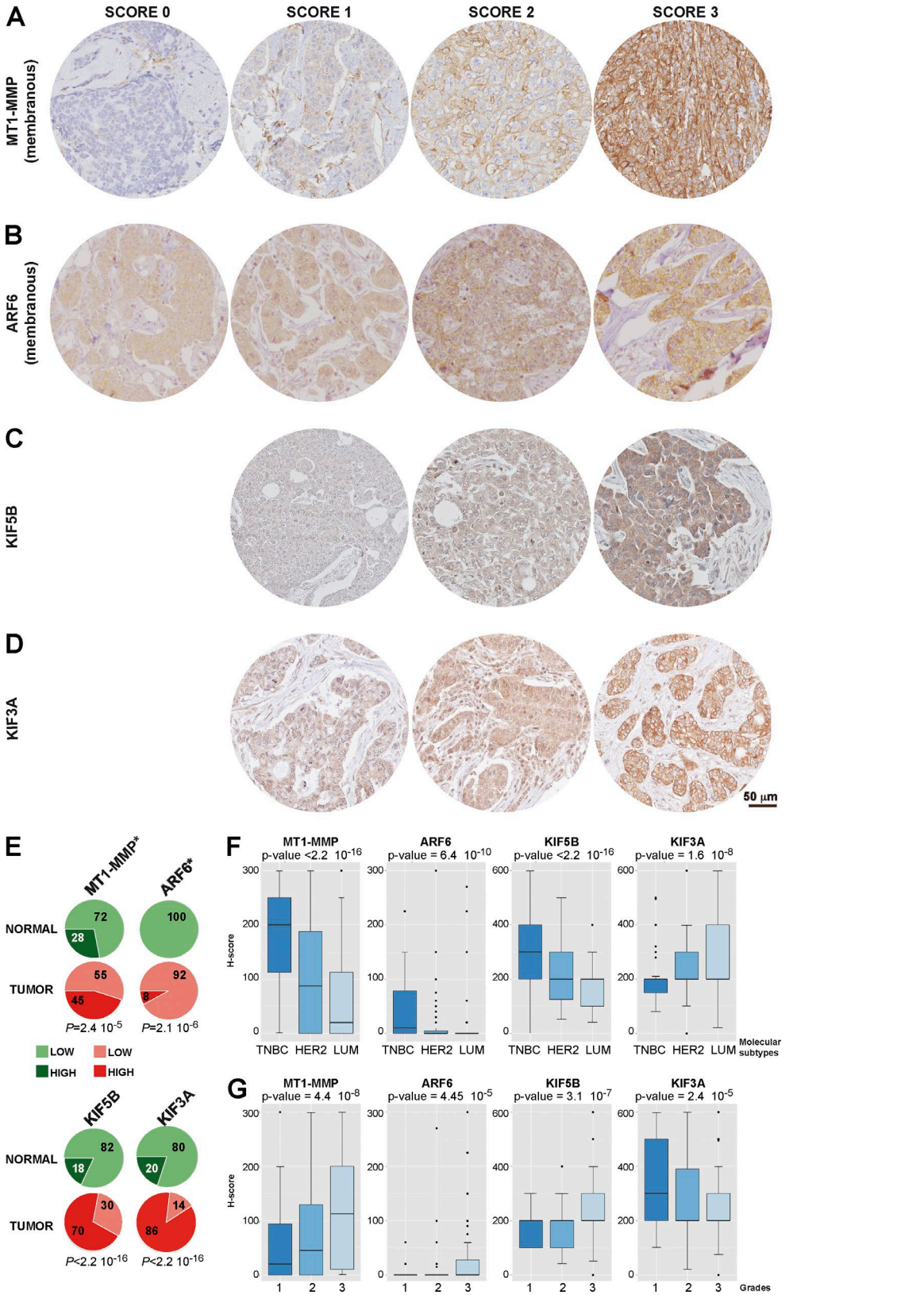

Figure 9. **Membranous ARF6 and MT1-MMP and KIF5B and KIF3A expression in breast cancer.** (A–D) Expression of membranous MT1-MMP (A), membranous ARF6 (B), KIF5B (C), and KIF3A (D) was measured by IHC on TMA (example of score assignment). (E) Expression of MT1-MMP, ARF6, KIF5B, and KIF3A segregated in low- and high-expression classes is significantly increased in tumor component of IDCs as compared with adjacent peritumoral area. Values are shown as percentage of total tumors. *, membranous signal was considered. (F and G) Box plot representation with maximum and minimum, 75th and 25th percentiles, and median values of H score of the different markers correlating with the molecular subtypes (F) and pathological grades (G). Analysis was performed on 311 cases for which scores were available for all four markers. ARF6 and MT1-MMP plasma membrane H scores and total (cytosol + plasma membrane) KIF5B and KIF3A H scores were considered.

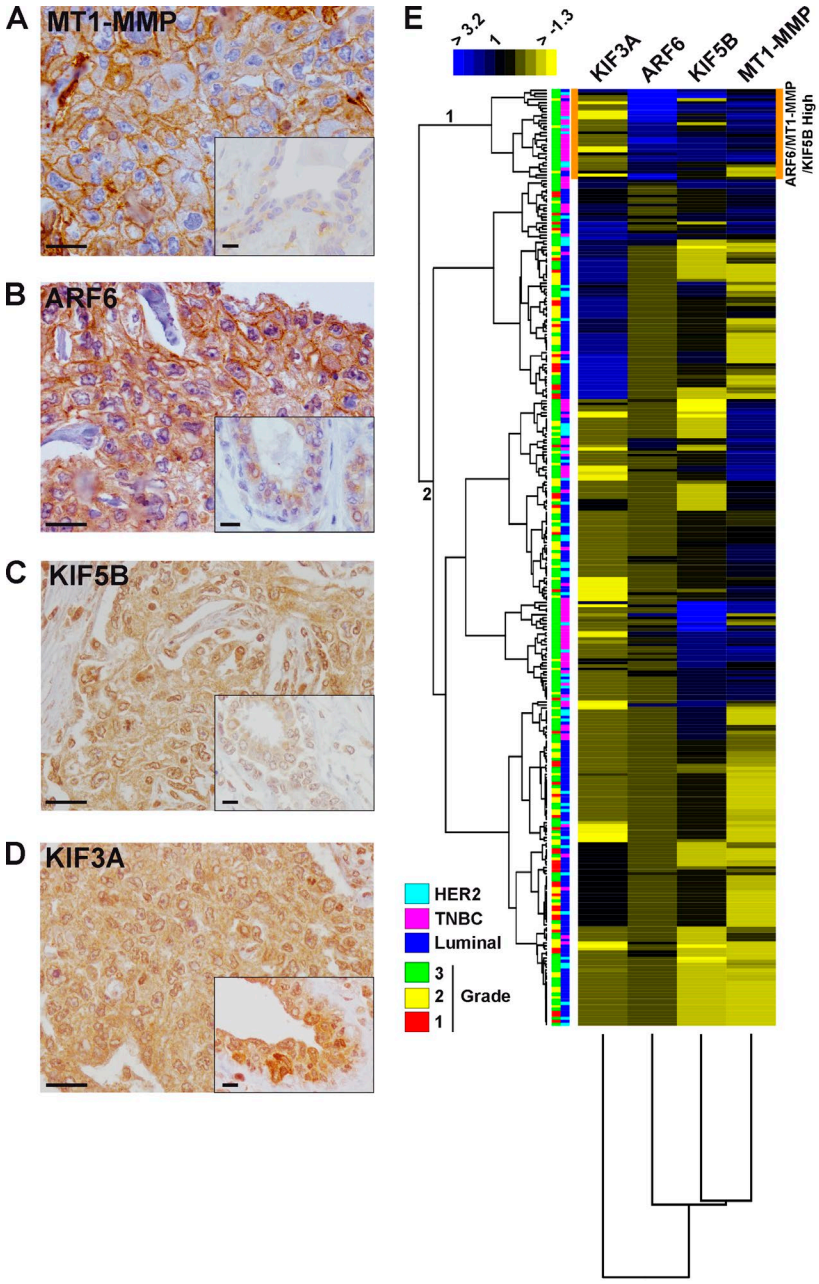

Figure 10. **ARF6, MT1-MMP, and KIF5B are up-regulated in TNBCs.** (A–D) IHC analysis of MT1-MMP, ARF6, KIF5B, and KIF3A in IDCs. Insets show the peritumoral area. Bars: 25 µm; (insets) 10 µm. (E) Hierarchical clustering of the staining patterns of 311 IDC samples based on total KIF3A and KIF5B, and membranous ARF6 and MT1-MMP expression. Data are shown in a table format with the vertical axis listing IDC samples and bars representing antibodies. A color scale, which represents relative staining patterns of each sample, is displayed at the top left corner. Molecular subtypes (HER2, TNBC, and Luminal A + B) and grades are depicted between clusters and dendrogram, with color coding annotated at the bottom left corner.

erate MDA-MB-231 cells stably expressing MT1-MMPmCh or -pHluorin, cells were transfected with Lipofectamine 2000 (Invitrogen) and selected with 800 µg/ml geneticin (Sakurai-Yageta et al., 2008) or 1 µg/ml puromycin (Lizárraga et al., 2009). MDA-MB-231 cells expressing H2B-GFP were retrovirally transduced with pBabe-puro/H2B-GFP and selected with 1 µg/ml puromycin (Castro-Castro et al., 2012). To generate KIF5B-YFP– and KIF3A-GFP–expressing cells, MDA-MB-231 cells stably expressing MT1-MMPmCh were transfected using Nucleofector (Lonza) according to the manufacturer's instructions, with 1 µg KIF5B-YFP or KIF3A-GFP plasmids and 100 ng of empty vector pBabe-puro vector, and selected by 1 µg/ml puromycin. Puromycin-resistant cells were sorted for GFP and mCherry expression. The MCF-10DCIS.com cell line was purchased from Asterand and maintained in DMEM-F12 medium with 5% horse serum.

siRNA treatment and lentiviral vectors for shRNA expression

siRNA treatments were performed using 50 nM siRNA (see Table S5 for the list of siRNAs) and Lullaby reagent (OZ Biosciences) according to the manufacturer's instructions and analyzed 72 h after treatment. shRNAs against human ARF6 and MT1-MMP inserted in pLKO.1-puro lentiviral vector were purchased from Sigma-Aldrich (Table S5). For lentivirus production, HEK293T cells were transfected using GeneJuice (EMD Millipore) with a mix of expression vector and psPAX2 (Addgene) and pVSV-G (Takara Bio Inc.) packaging vectors in OPTIMEM medium (Invitrogen). After 72 h, the virus-containing supernatant was collected, filtered, and used for transduction of a subconfluent monolayer of MDA-MB-231 or MCF10DCIS.com cells. 1 µg/ml puromycin (Gibco) was added after 48 h for selection.

Indirect IF and confocal microscopy

To visualize endogenous motors and JIP4 association to MT1-MMP–positive endosomes, MDA-MB-231 cells stably expressing MT1-MMPmCh were cultured on gelatin-coated coverslips, prepermeabilized with 0.5% Triton X-100 in a microtubule-stabilizing buffer (4% PFA, 100 mM Pipes, pH 6.9, 10 µM taxol, and 1 mM EGTA) for 2 min, and then fixed in a microtubule-stabilizing buffer for 20 min at 37°C. Then, cells were washed in PBS and stained with primary antibodies (Table S4) and counterstained with appropriate Alexa Fluor 488– and Cy5-conjugated secondary antibodies (Molecular Probes). For confocal microscopy analysis, an image acquisition was performed with a confocal microscope (A1R; Nikon) with a 60× oil objective, and a z-dimension series of images was taken every 0.5 µm.

3D deconvolution microscopy

For 3D deconvolution analysis, images were acquired with a wide-field microscope (Eclipse 90i Upright; Nikon) using a 100× Plan Apo VC 1.4 oil objective and a highly sensitive cooled interlined charge-coupled device (CCD) camera (CoolSNAP HQ2; Roper Scientific). A z-dimension series of images was taken every 0.2 µm by means of a piezoelectric motor (Physik Instrumente), and images were deconvoluted (Sibarita, 2005). To quantify the association of motor proteins to MT1-MMP endosomes, a motor association index was calculated based on segmentation of MT1-MMPmCh–positive endosomes by the thresholding of deconvoluted images. Then, the number of dots of motor proteins associated with each segmented object (MT1-MMP–positive endosomes) was scored using a "particle counting inside regions of interest" macro in ImageJ. The number of dots was normalized to the total number of dots for each motor protein per cell (Motor Association Index) by setting the index of siNT-treated cells to 100.

PLA

For PLA (Söderberg et al., 2006), MDA-MB-231 cells stably expressing MT1-MMPpHluorin grown on coverslips coated with cross-linked gelatin were permeabilized with 0.5% Triton X-100 in 4% PFA, fixed in 4% PFA, and then incubated with the primary antibodies rabbit polyclonal anti-JIP4 and mouse monoclonal anti-$p150^{Glued}$. Secondary antibodies tagged with short DNA oligonucleotides were added. Hybridization, ligation, amplification, and detection were realized according to the manufacturer's protocol (Olink Bioscience). In brief, secondary antibodies were incubated in a preheated humidity chamber for 1 h at 37°C. Ligation was performed with a ligase-containing ligation solution for 30 min at 37°C. Then, the amplification step was performed with a polymerase-containing amplification solution for 100 min at 37°C. Finally, coverslips were incubated with Cy3-conjugated IgGs to detect a Duolink signal. JIP4-$p150^{Glued}$ Duolink signal staining was measured by counting the number of red dots for each cell from 3D deconvoluted images with a "find maxima" plugin of ImageJ software and compared with control conditions in which JIP3 + JIP4 was depleted (si$JIP3^{\#3}$ + $JIP4^{\#4}$) or one of the primary antibodies was omitted.

Analysis of endosome distribution

Software has been developed in MATLAB to study the relative position of MT1-MMPmCh endosomes to the cell centroid (Castro-Castro et al., 2012). First, cells are automatically segmented from the phase-contrast image. A polar coordinate system is created, where the main (longest) axis of the cell becomes the 0–180° axis with the cell centroid as the center. Vesicles are then automatically segmented from the matching fluorescence image using a Laplacian of Gaussian filter and mathematical morphology. Each vesicle is then expressed in the cell polar coordinate system, where its radius is expressed relative to the length of the line going from the cell centroid through the vesicle centroid to the cell periphery. Segmentation was manually corrected as needed. Results are represented by classes according to the distance between each MT1-MMP segmented vesicle and the cell centroid (expressed as the percentage of the total distance between the cell centroid and the cell periphery).

Fluorescent gelatin degradation assay

FITC-labeled gelatin was obtained from Invitrogen. In brief, coverslips (18-mm diameter) were coated with 0.5 µg/ml (MDA-MB-231 cells/MCF10DCIS.com cells) or 50 µg/ml poly-L-lysine (MDA-MB-231 cells stably expressing MT1MMPmCh and KIF5B-YFP) for 20 min at RT, washed with PBS, and fixed with 0.5% glutaraldehyde (Sigma-Aldrich) for 15 min. After three washes, the coverslips were inverted on an 80-µl drop of 0.2% fluorescently labeled gelatin in 2% sucrose in PBS and incubated for 10 min at RT. After washing with PBS, coverslips were incubated in 5 mg/ml sodium borohydride for 3 min, washed three times in PBS, and finally incubated in 2 ml of complete medium for a minimum of 30 min before adding the cells. To assess the ability of the cells to form invadopodia and degrade the matrix, 7×10^4 cells per 12 wells were plated on fluorescent gelatin-coated coverslips and incubated at 37°C for 12 h (MCF10DICS.com cells), 5 h (MDA-MB-231 cells), or 2 h (MDA-MB-231 cells stably expressing MT1-MMPmCh and KIF5B-YFP). Cells were then prepermeabilized with 0.5% Triton X-100 in 4% PFA for 90 s, fixed with 4% PFA for 20 min at RT, quenched with 50 mM NH_4Cl for 10 min, and processed for intracellular IF labeling with Alexa Fluor 594–phalloidin or paxillin as indicated. Cells were imaged with a 63× objective (NA 1.40 differential interference contrast [DIC] oil) of a wide-field microscope (DM6000 B/M; Leica) equipped with a CCD camera (CoolSNAP HQ) controlled by MetaMorph software (Molecular Devices). For the quantification of degradation, the total area of degraded matrix in one field (black pixels), measured using the Threshold command of MetaMorph 6.2.6, was divided by the total number of phalloidin-labeled cells in the field to define a degradation index.

Invasion of multicellular spheroids in 3D type I collagen

Multicellular spheroids of MDA-MB-231 cells were prepared with the hanging droplet method (Kelm et al., 2003), using 3×10^3 cells in a 20-µl droplet in a complete L15 medium. For siRNA treatment, cells were transfected by nucleofection (Kit V; Lonza) with 50-nM siRNAs as indicated. After nucleofection, cells were plated in a Petri dish and the day after were transfected again with 50 nM of each siRNA by using Lullaby reagent (OZ Biosciences), according to the manufacturer's protocol, for 6 h. Spheroids were made immediately after this second round of siRNA transfection. After 3 d, spheroids were embedded in type I collagen (prepared from acid extracts of rat tail tendon at a final concentration of 2.2 mg/ml; Elsdale and Bard, 1972). Spheroids were fixed in 4% PFA immediately after polymerization of the matrix (T0) or after 2 d of invasion (T2). After fixation, cells in spheroids were permeabilized for 15 min in 0.1% Triton X-100/PBS and labeled with Alexa Fluor 594–phalloidin and DAPI.

For quantification of invasion in 3D type I collagen matrix, phalloidin-labeled spheroids were imaged at RT with a confocal microscope (A1R) using a 10× CFI Plan objective (NA 0.25 working distance [WD] 7-mm DIC Dry), steered by NIS Elements software (Nikon) and collecting a stack of images along the z axis with a 10-µm interval between optical stions. The spheroid mean diameter was measured from azimuthal averaging of intensity profile along a line centered on the spheroid using a homemade plugin in ImageJ software (Rey et al., 2011). Averaging consists in measuring intensity profiles along a rotating line by 5° steps and calculating the mean value over all angles of each pixel of the line. The mean diameter was then taken as

the width at 1/10 of the maximal value of these mean intensity profiles. Mean area (πr^2) was calculated from the mean diameter.

Circular cell invasion assay

Invasive migration in 3D collagen I was assessed using the Oris Cell Invasion Assay (Platypus Technologies). H2B-EGFP–expressing MDA-MB-231 cells were reverse transfected with Lullaby reagent (OZ Bioscience) with 50 nM of each siRNA. 24 h after transfection, cells were trypsinized, counted, and 4×10^4 cells per well were seeded in the presence of Oris Cell Seeding Stoppers to restrict seeding to the outer annular regions of the wells in a 96-well plate coated with a type I collagen bottom layer. Removal of the stoppers revealed a 2-mm-diameter unseeded region in the center of each well (i.e., the detection zone), into which the seeded cells may then invade for a 48-h time period once a collagen I overlay has been applied. Type I collagen was prepared from acid extracts of rat tail tendon at a final concentration of 2.2 mg/ml (Elsdale and Bard, 1972). H2B-EGFP images were acquired at 37°C from each well at the beginning (T0) and 48 h after invasion (T2) using a microscope (TE2000; Nikon) equipped with a CFI 4× objective Plan Fluor (NA 0.13 WD 30-mm DIC Dry) controlled by MetaMorph software. This microscope was equipped with a cooled CCD camera (HQ2; Roper Scientific).

Image analysis was performed using MetaMorph software. The invasion index was determined by thresholding the area occupied by H2B-EGFP nuclei in the detection zone of each well after 48 h of invasion. This index is defined as the total area occupied by H2B-GFP nuclei in the unseeded area (detection zone) at the end of the assay (T2) by subtracting the area occupied by H2B-GFP nuclei at the beginning of the experiment (T0). This area of invasion was normalized, and the results from three independent experiments are represented.

Quantification of pericellular collagenolysis

Cells treated with 50 nM of indicated siRNAs were trypsinized and resuspended in 0.2 ml of 2.2 mg/ml collagen I solution (2.5×10^5 cells/ml) loaded on a glass coverslip. After gelling for 30 min at 37°C, a complete L15 medium was added, and collagen-embedded cells were incubated for 24 h at 37°C in 1% CO_2. After fixation in 4% PFA in PBS at 37°C for 30 min, samples were incubated with 2.5 µg/ml anti–Col1-$^{3/4C}$ antibodies for 2 h at 4°C, washed extensively with PBS, and counterstained with Cy3-conjugated anti–rabbit IgG antibodies, DAPI, and Alexa Fluor 488–phalloidin to see the cell shape. Image acquisition was performed at RT with a confocal microscope (A1R) with a CFI 40× Plan Fluor objective (NA 1.3 WD 0.65 DIC oil) controlled by NIS Elements software. Quantification of degradation spots was performed with a homemade ImageJ macro (Monteiro et al., 2013). Images were preprocessed by a Laplacian of Gaussian filter (Sage et al., 2005), with the variance reflecting the expected spot size. The spot detection then consisted of finding the local minima, sorting them in ascending order of intensity, applying a flood-fill algorithm to each of them using a fixed noise-tolerance value setup for all experiments at 10,000 fluorescence intensity arbitrary unit, and discarding higher minima whose fill regions touch those of lower minima. Detected spots are then counted and saved for visual verification. No manual correction was done. The degradation index is the number of degradation spots divided by the number of cells present in the field, normalized to the degradation index of control cells set to 100.

MT1-MMPpHluorin exocytosis on collagen type I fibers

MDA-MB-231 cells stably expressing MT1-MMPpHluorin were treated with the indicated siRNAs for 72 h and plated on MatTek dishes layered with a drop of polymerized type I collagen mixed with Alexa Fluor 549–conjugated type I collagen (10% final) at a final concentration of 2.5 mg/ml. Cells were incubated for 30 min at 37°C in 1% CO_2 and imaged (2 z stacks/min for a 30-min period) at 37°C on a complete L15 medium by multicolor confocal spinning disk microscopy using a spinning disk microscope (Roper Scientific) based on a CSU22 head (Yokogawa) mounted on the lateral port of an inverted microscope (TE-2000U; Nikon) equipped with a 60× 1.45 NA oil-immersion objective, a PIFOC Objective stepper, and a dual output laser launch that included 491- and 561-nm 50-mW DPSS lasers (Roper Scientific). Images were acquired with a CCD camera (CoolSNAP HQ2) and steered by MetaMorph software. The number of exocytic events of MT1-MMPpHluorin (i.e., GFP flashes) was manually measured per minute and per cell.

TIRF microscopy and live cell spinning disk confocal microscopy

For live cell TIRF microscopy, MDA-MB-231 cells stably expressing MT1-MMPmCh and KIF5B-YFP were plated on glass-bottom dishes (MatTek Corporation), coated with cross-linked gelatin, and imaged with a 100-ms exposure time at 2-s intervals for 30 s through a 100× 1.49 NA TIRF objective on an inverted microscope (TE2000; Nikon) equipped with a QuantEM EMCCD camera (Roper Scientific), a dual output laser launch that included 491- and 561-nm 50-mW DPSS lasers (Roper Scientific), and driven by MetaMorph software. A motorized device driven by MetaMorph allowed the accurate positioning of the illumination light for evanescent wave excitation.

For live cell confocal spinning disk microscopy, MDA-MB-231 cells stably expressing MT1-MMPmCh and YFP, KIF5B-YFP, or KIF3A-GFP were plated on glass-bottom dishes (MatTek Corporation) coated with cross-linked gelatin and kept in a humidified atmosphere at 37°C in 1% CO_2. The movement of MT1-MMPmCh vesicles was monitored by acquiring 3D time-series images by confocal spinning disk microscopy (1 z stack/2 s for a period of 1 min, or 1 z stack/3 s for a duration of 3 min) using a spinning disk microscope (Roper Scientific) based on a CSU22 head mounted on the lateral port of an inverted microscope (TE-2000U) equipped with a 60× 1.45 NA oil-immersion objective, a PIFOC Objective stepper, and a dual output laser launch that included 491- and 561-nm 50-mW DPSS lasers (Roper Scientific). Images were acquired with a CCD camera (CoolSNAP HQ2) and steered by MetaMorph software. To quantify the motility of MT1-MMP endosomes, we determined a displacement index (Quintero et al., 2009) obtained by dividing the area over which the MT1-MMPmCh endosomes moved in a 1-min time lapse (as a result of the time-lapse projection of the 31 frames recorded every 2 s) by the area occupied by MT1-MMP endosomes in the first frame of the time sequence (see Fig. S4 D). To quantify MT1-MMPmCh endosome tubulation, time-lapse sequences comprising 61 frames were acquired with a 3-s time interval. The number of elongating endosomes was scored in a 100-pixel size region at the cell periphery of every sixth frame from the time-lapse sequences (11 frames total). The tubulation index was defined as the number of tubules scored per frame per cell surface area analyzed.

Immunoprecipitation and immunoblotting analysis

For immunoprecipitation analysis, MDA-MB-231 cells stably expressing MT1-MMPmCh treated with the indicated siRNAs or stably expressing YFP, KIF5B-YFP, or KIF3A-GFP were lysed in 50-mM Tris, pH 7.4, 150-mM NaCl, 10-mM $MgCl_2$, 10% glycerol, and 1% NP-40 with protease inhibitors for 30 min and centrifuged at 13,000 rpm for 10 min at 4°C. Supernatants were incubated with 15 µl RFP- or GFP-Trap–coupled agarose beads (ChromoTek) for 2 h at 4°C. Beads were washed three times in lysis buffer, and bound proteins were eluted in SDS sample buffer and analyzed by SDS-PAGE and immunoblotting with indicated antibodies (Table S4). Bound antibodies were detected with ECL Western Blotting Detection Reagents (GE Healthcare) and revealed by autoradiographical film (GE Healthcare) or CCD camera (Bio-Rad Laboratories).

IHC analysis of breast cancer TMA

Analysis of human samples was performed in accordance with French Bioethics Law 2011–814, the French National Institute of Cancer Ethics Charter, and after approval by the Institut Curie Review Board and Ethics committee (Comité de Pilotage du Groupe Sein), which waived the need for written informed consent from the participants. Women were informed of the research use of their tissues and did not declare any opposition to such research. Data were analyzed anonymously. Samples of primary breast tumors surgically removed before any radiation, hormonal, or chemotherapy treatment at Institut Curie from 2005 to 2006 have been analyzed. Alcohol formalin acetic acid–fixed paraffin-embedded samples comprised all of the TNBC and HER2 tumors available, as well as an equal number of consecutively treated luminal tumors. Based on clinicopathology, tumors were classified as IDC and/or DCIS. Breast molecular subtypes were defined as follows: luminal, ER ≥ 10%, PR ≥ 20%; HER2+: ER– PR– HER2+, ER < 10%, PR < 10%, HER2 2+ amplified or 3+; ER– PR– HER2– (TNBCs), ER < 10%, PR < 10%, HER2 0/1+ or 2+ nonamplified according to the ASCO guidelines. Inclusion of DCIS and tumors followed the same criteria as IDCs.

TMA consisted of replicate 1-mm-diameter tumor cores selected from whole-tumor tissue stion in the most representative tumor areas (high tumor cell density) of each tumor sample and a matched tissue core from adjacent nontumoral breast epithelium. For IHC staining, an EnVision FLEX, High pH kit (Dako) was used according to the manufacturer's instructions. IHC labeling intensity in carcinoma cells was scored using marker-specific 0–3 scales (see Fig. 9, A–D) and multiplied by the percentage of positive cells (H score). The average H score of duplicate tissue cores was calculated. Distribution of H-score values for each marker according to breast cancer subtype and tumor grade was compared by an analysis of variance test and plotted using the ggplot2 R package. IHC H scores were scaled and analyzed by unsupervised hierarchical clustering using the Ward linkage-clustering algorithm with euclidean distance as the similarity metric using R Software (version 3.1.1). H-score variables were discretized either in low or high expression in order to perform the association test (Table S2). Cut-off values for IHC H scores were calculated using normal mixture modeling (Mclust R package). For MT1-MMP and ARF6, we used membranous H scores with a threshold estimated at 100. For KIF5B and KIF3A, total H scores (the sum of membranous and cytoplasmic IHC H scores) were used, and the threshold was estimated at 200. H scores were compared between groups by the χ^2 test or Fisher's exact test when appropriate using R Software. P-values ≤ 0.05 were considered statistically significant (Table S3).

Statistics

Except for the IHC data of tumor specimens, statistical analyses were performed using the Mann-Whitney *t* test, one-way or two-way analysis of variance, and χ^2 test, using GraphPad Prism (GraphPad Software) with $P < 0.05$ considered significant.

Online supplemental material

Fig. S1 shows the depletion of ARF6 by three independent siRNAs and the effect of ARF6 knockdown on the invasion potential of MCF10DCIS.com cells. Fig. S2 shows the effect of JIP3 and JIP4 knockdown on 3D invasion and matrix degradation by MDA-MB-231 cells. Fig. S3 shows that depletion of ARF6 or JIP3/JIP4 does not affect early or late endosomal maturation, whereas it impairs MT1-MMP exocytosis. Fig. S4 shows the specificity of KIF5B, KIF3A, and $p150^{Glued}$ antibodies and the effect of KIF5B and KIF3A overexpression on MT1-MMP endosome positioning and movement. Fig. S5 documents the effect of ARF6, JIP3/JIP4, and $p150^{Glued}$ knockdown on matrix degradation. Table S1 details the characteristics of primary breast tumors analyzed by IHC in the TMA. Table S2 compares membranous MT1-MMP, ARF6, KIF5B, and KI3A expression in invasive breast cancers. Table S3 provides P-values of χ^2 test corresponding to Table S2. Tables S4 and S5 provide a list of antibodies and si/shRNAs used in this study. Video 1 shows the effect of ARF6 and JIP3/JIP4 silencing on MT1-MMP endosome dynamics and positioning. Video 2 illustrates the implication of kinesin-2/KIF3A in peripheral MT1-MMP endosome distribution in cells knocked down for JIP3 and JIP4. Video 3 shows the requirement for JIP3/JIP4 and $p150^{Glued}$ in MT1-MMP endosomal tabulation. Online supplemental material is available at http://www.jcb.org/cgi/content/full/jcb.201506002/DC1.

Acknowledgments

Dr. G.M. Griffiths is acknowledged for critical reading of the manuscript. We thank the Breast Cancer Study Group and patients of Institut Curie for breast tumor samples and the Nikon Imaging Centre at Institut Curie–Centre National pour la Recherche Scientifique (CNRS), CNRS and Cell and Tissue Imaging Facility of Institut Curie, and members of the France Bio Imaging national research infrastructure (ANR-10-INSB-04) for help with image acquisition. Dr. A. Soltani is acknowledged for contributing to pilot experiments, Dr. C. Laurent for help with IHC dataset analysis, Dr. P. Paul-Gilloteaux for help with endosome position analysis, and A. Kawska (IlluScientia.com) for artwork in Fig. 7 (F and G). Dr. A. Houdusse is acknowledged for help with the ARF6/JIP4 3D structure used in Fig. 7 G.

V. Marchesin was supported by fellowships from Domaine d'Intérêt Majeur de la Région Ile-de-France and Ligue Nationale contre le Cancer; A. Castro-Castro by a Long-Term European Molecular Biology Organization fellowship; C. Lodillinsky by a postdoctoral fellowship from Fondation Pierre-Gilles de Gennes pour la Recherche; J. Cyrta by an MD Master 2 fellowship from Institut Curie; E. Infante by a postdoctoral fellowship from Ligue Nationale contre le Cancer; and L. Fuhrmann and M. Irondelle by the incentive and cooperative research program "Breast Cancer: Cell Invasion and Motility" of Institut Curie. Funding for this work was provided by grants from Ligue Nationale Contre le Cancer (Equipe Labellisée 2015) and Institut National du Cancer (2012-1-PL BIO-02-IC-1) to P. Chavrier and by core funding from Institut Curie and CNRS.

The authors declare no competing financial interests.

Submitted: 30 May 2015
Accepted: 15 September 2015

References

Artym, V.V., Y. Zhang, F. Seillier-Moiseiwitsch, K.M. Yamada, and S.C. Mueller. 2006. Dynamic interactions of cortactin and membrane type 1 matrix metalloproteinase at invadopodia: defining the stages of invadopodia formation and function. *Cancer Res.* 66:3034–3043. http://dx.doi.org/10.1158/0008-5472.CAN-05-2177

Bonnans, C., J. Chou, and Z. Werb. 2014. Remodelling the extracellular matrix in development and disease. *Nat. Rev. Mol. Cell Biol.* 15:786–801. http://dx.doi.org/10.1038/nrm3904

Bowman, A.B., A. Kamal, B.W. Ritchings, A.V. Philp, M. McGrail, J.G. Gindhart, and L.S. Goldstein. 2000. Kinesin-dependent axonal transport is mediated by the sunday driver (SYD) protein. *Cell.* 103:583–594. http://dx.doi.org/10.1016/S0092-8674(00)00162-8

Castro-Castro, A., C. Janke, G. Montagnac, P. Paul-Gilloteaux, and P. Chavrier. 2012. ATAT1/MEC-17 acetyltransferase and HDAC6 deacetylase control a balance of acetylation of alpha-tubulin and cortactin and regulate MT1-MMP trafficking and breast tumor cell invasion. *Eur. J. Cell Biol.* 91:950–960. http://dx.doi.org/10.1016/j.ejcb.2012.07.001

Cavalli, V., P. Kujala, J. Klumperman, and L.S. Goldstein. 2005. Sunday Driver links axonal transport to damage signaling. *J. Cell Biol.* 168:775–787. http://dx.doi.org/10.1083/jcb.200410136

Coschi, C.H., A.L. Martens, K. Ritchie, S.M. Francis, S. Chakrabarti, N.G. Berube, and F.A. Dick. 2010. Mitotic chromosome condensation mediated by the retinoblastoma protein is tumor-suppressive. *Genes Dev.* 24:1351–1363. http://dx.doi.org/10.1101/gad.1917610

D'Souza-Schorey, C., and P. Chavrier. 2006. ARF proteins: roles in membrane traffic and beyond. *Nat. Rev. Mol. Cell Biol.* 7:347–358. http://dx.doi.org/10.1038/nrm1910

Derivery, E., E. Helfer, V. Henriot, and A. Gautreau. 2012. Actin polymerization controls the organization of WASH domains at the surface of endosomes. *PLoS One.* 7:e39774. http://dx.doi.org/10.1371/journal.pone.0039774

Donaldson, J.G., and C.L. Jackson. 2011. ARF family G proteins and their regulators: roles in membrane transport, development and disease. *Nat. Rev. Mol. Cell Biol.* 12:362–375. http://dx.doi.org/10.1038/nrm3117

Elsdale, T., and J. Bard. 1972. Collagen substrata for studies on cell behavior. *J. Cell Biol.* 54:626–637. http://dx.doi.org/10.1083/jcb.54.3.626

Gomez, T.S., J.A. Gorman, A.A. de Narvajas, A.O. Koenig, and D.D. Billadeau. 2012. Trafficking defects in WASH-knockout fibroblasts originate from collapsed endosomal and lysosomal networks. *Mol. Biol. Cell.* 23:3215–3228. http://dx.doi.org/10.1091/mbc.E12-02-0101

Granger, E., G. McNee, V. Allan, and P. Woodman. 2014. The role of the cytoskeleton and molecular motors in endosomal dynamics. *Semin. Cell Dev. Biol.* 31:20–29. http://dx.doi.org/10.1016/j.semcdb.2014.04.011

Hancock, W.O. 2014. Bidirectional cargo transport: moving beyond tug of war. *Nat. Rev. Mol. Cell Biol.* 15:615–628. http://dx.doi.org/10.1038/nrm3853

Hashimoto, S., Y. Onodera, A. Hashimoto, M. Tanaka, M. Hamaguchi, A. Yamada, and H. Sabe. 2004. Requirement for Arf6 in breast cancer invasive activities. *Proc. Natl. Acad. Sci. USA.* 101:6647–6652. http://dx.doi.org/10.1073/pnas.0401753101

Hashimoto, S., M. Hirose, A. Hashimoto, M. Morishige, A. Yamada, H. Hosaka, K. Akagi, E. Ogawa, C. Oneyama, T. Agatsuma, et al. 2006. Targeting AMAP1 and cortactin binding bearing an atypical src homology 3/proline interface for prevention of breast cancer invasion and metastasis. *Proc. Natl. Acad. Sci. USA.* 103:7036–7041. http://dx.doi.org/10.1073/pnas.0509166103

Hoshino, D., K.C. Kirkbride, K. Costello, E.S. Clark, S. Sinha, N. Grega-Larson, M.J. Tyska, and A.M. Weaver. 2013. Exosome secretion is enhanced by invadopodia and drives invasive behavior. *Cell Reports.* 5:1159–1168. http://dx.doi.org/10.1016/j.celrep.2013.10.050

Hotary, K., X.Y. Li, E. Allen, S.L. Stevens, and S.J. Weiss. 2006. A cancer cell metalloprotease triad regulates the basement membrane transmigration program. *Genes Dev.* 20:2673–2686. http://dx.doi.org/10.1101/gad.1451806

Hotary, K.B., E.D. Allen, P.C. Brooks, N.S. Datta, M.W. Long, and S.J. Weiss. 2003. Membrane type I matrix metalloproteinase usurps tumor growth control imposed by the three-dimensional extracellular matrix. *Cell.* 114:33–45. http://dx.doi.org/10.1016/S0092-8674(03)00513-0

Hu, M., J. Yao, D.K. Carroll, S. Weremowicz, H. Chen, D. Carrasco, A. Richardson, S. Violette, T. Nikolskaya, Y. Nikolsky, et al. 2008. Regulation of in situ to invasive breast carcinoma transition. *Cancer Cell.* 13:394–406. http://dx.doi.org/10.1016/j.ccr.2008.03.007

Huang, J., A.J. Roberts, A.E. Leschziner, and S.L. Reck-Peterson. 2012. Lis1 acts as a "clutch" between the ATPase and microtubule-binding domains of the dynein motor. *Cell.* 150:975–986. http://dx.doi.org/10.1016/j.cell.2012.07.022

Isabet, T., G. Montagnac, K. Regazzoni, B. Raynal, F. El Khadali, P. England, M. Franco, P. Chavrier, A. Houdusse, and J. Ménétrey. 2009. The structural basis of Arf effector specificity: the crystal structure of ARF6 in a complex with JIP4. *EMBO J.* 28:2835–2845. http://dx.doi.org/10.1038/emboj.2009.209

Kelkar, N., S. Gupta, M. Dickens, and R.J. Davis. 2000. Interaction of a mitogen-activated protein kinase signaling module with the neuronal protein JIP3. *Mol. Cell. Biol.* 20:1030–1043. http://dx.doi.org/10.1128/MCB.20.3.1030-1043.2000

Kelm, J.M., N.E. Timmins, C.J. Brown, M. Fussenegger, and L.K. Nielsen. 2003. Method for generation of homogeneous multicellular tumor spheroids applicable to a wide variety of cell types. *Biotechnol. Bioeng.* 83:173–180. http://dx.doi.org/10.1002/bit.10655

King, S.J., and T.A. Schroer. 2000. Dynactin increases the processivity of the cytoplasmic dynein motor. *Nat. Cell Biol.* 2:20–24. http://dx.doi.org/10.1038/71338

Lizárraga, F., R. Poincloux, M. Romao, G. Montagnac, G. Le Dez, I. Bonne, G. Rigaill, G. Raposo, and P. Chavrier. 2009. Diaphanous-related formins are required for invadopodia formation and invasion of breast tumor cells. *Cancer Res.* 69:2792–2800. http://dx.doi.org/10.1158/0008-5472.CAN-08-3709

Lodillinsky, C., E. Infante, A. Guichard, R. Chaligné, L. Fuhrmann, J. Cyrta, M. Irondelle, E. Lagoutte, S. Vacher, H. Bonsang-Kitzis, et al. 2015. p63/MT1-MMP axis is required for in situ to invasive transition in basal-like breast cancer. *Oncogene.* http://dx.doi.org/10.1038/onc.2015.87

McKenney, R.J., M. Vershinin, A. Kunwar, R.B. Vallee, and S.P. Gross. 2010. LIS1 and NudE induce a persistent dynein force-producing state. *Cell.* 141:304–314. http://dx.doi.org/10.1016/j.cell.2010.02.035

McKenney, R.J., W. Huynh, M.E. Tanenbaum, G. Bhabha, and R.D. Vale. 2014. Activation of cytoplasmic dynein motility by dynactin-cargo adapter complexes. *Science.* 345:337–341. http://dx.doi.org/10.1126/science.1254198

Montagnac, G., J.B. Sibarita, S. Loubéry, L. Daviet, M. Romao, G. Raposo, and P. Chavrier. 2009. ARF6 Interacts with JIP4 to control a motor switch mechanism regulating endosome traffic in cytokinesis. *Curr. Biol.* 19:184–195. http://dx.doi.org/10.1016/j.cub.2008.12.043

Monteiro, P., C. Rossé, A. Castro-Castro, M. Irondelle, E. Lagoutte, P. Paul-Gilloteaux, C. Desnos, E. Formstecher, F. Darchen, D. Perrais, et al. 2013. Endosomal WASH and exocyst complexes control exocytosis of MT1-MMP at invadopodia. *J. Cell Biol.* 203:1063–1079. http://dx.doi.org/10.1083/jcb.201306162

Morishige, M., S. Hashimoto, E. Ogawa, Y. Toda, H. Kotani, M. Hirose, S. Wei, A. Hashimoto, A. Yamada, H. Yano, et al. 2008. GEP100 links epidermal growth factor receptor signalling to Arf6 activation to induce breast cancer invasion. *Nat. Cell Biol.* 10:85–92. http://dx.doi.org/10.1038/ncb1672

Neve, R.M., K. Chin, J. Fridlyand, J. Yeh, F.L. Baehner, T. Fevr, L. Clark, N. Bayani, J.P. Coppe, F. Tong, et al. 2006. A collection of breast cancer cell lines for the study of functionally distinct cancer subtypes. *Cancer Cell.* 10:515–527. http://dx.doi.org/10.1016/j.ccr.2006.10.008

Nguyen, Q., C.M. Lee, A. Le, and E.P. Reddy. 2005. JLP associates with kinesin light chain 1 through a novel leucine zipper-like domain. *J. Biol. Chem.* 280:30185–30191. http://dx.doi.org/10.1074/jbc.M505499200

Onodera, Y., S. Hashimoto, A. Hashimoto, M. Morishige, Y. Mazaki, A. Yamada, E. Ogawa, M. Adachi, T. Sakurai, T. Manabe, et al. 2005. Expression of AMAP1, an ArfGAP, provides novel targets to inhibit breast cancer invasive activities. *EMBO J.* 24:963–973. http://dx.doi.org/10.1038/sj.emboj.7600588

Onodera, Y., J.M. Nam, A. Hashimoto, J.C. Norman, H. Shirato, S. Hashimoto, and H. Sabe. 2012. Rab5c promotes AMAP1-PRKD2 complex formation to enhance β1 integrin recycling in EGF-induced cancer invasion. *J. Cell Biol.* 197:983–996. http://dx.doi.org/10.1083/jcb.201201065

Perentes, J.Y., N.D. Kirkpatrick, S. Nagano, E.Y. Smith, C.M. Shaver, D. Sgroi, I. Garkavtsev, L.L. Munn, R.K. Jain, and Y. Boucher. 2011. Cancer cell-associated MT1-MMP promotes blood vessel invasion and distant metastasis in triple-negative mammary tumors. *Cancer Res.* 71:4527–4538. http://dx.doi.org/10.1158/0008-5472.CAN-10-4376

Poincloux, R., F. Lizárraga, and P. Chavrier. 2009. Matrix invasion by tumour cells: a focus on MT1-MMP trafficking to invadopodia. *J. Cell Sci.* 122:3015–3024. http://dx.doi.org/10.1242/jcs.034561

Quintero, O.A., M.M. DiVito, R.C. Adikes, M.B. Kortan, L.B. Case, A.J. Lier, N.S. Panaretos, S.Q. Slater, M. Rengarajan, M. Feliu, and R.E. Cheney. 2009. Human Myo19 is a novel myosin that associates with mitochondria. *Curr. Biol.* 19:2008–2013. http://dx.doi.org/10.1016/j.cub.2009.10.026

Rey, M., M. Irondelle, F. Waharte, F. Lizarraga, and P. Chavrier. 2011. HDAC6 is required for invadopodia activity and invasion by breast tumor cells. *Eur. J. Cell Biol.* 90:128–135. http://dx.doi.org/10.1016/j.ejcb.2010.09.004

Rossé, C., C. Lodillinsky, L. Fuhrmann, M. Nourieh, P. Monteiro, M. Irondelle, E. Lagoutte, S. Vacher, F. Waharte, P. Paul-Gilloteaux, et al. 2014. Control of MT1-MMP transport by atypical PKC during breast-cancer progression. *Proc. Natl. Acad. Sci. USA.* 111:E1872–E1879. http://dx.doi.org/10.1073/pnas.1400749111

Sabe, H., S. Hashimoto, M. Morishige, E. Ogawa, A. Hashimoto, J.M. Nam, K. Miura, H. Yano, and Y. Onodera. 2009. The EGFR-GEP100-Arf6-AMAP1 signaling pathway specific to breast cancer invasion and metastasis. *Traffic.* 10:982–993. http://dx.doi.org/10.1111/j.1600-0854.2009.00917.x

Sage, D., F.R. Neumann, F. Hediger, S.M. Gasser, and M. Unser. 2005. Automatic tracking of individual fluorescence particles: application to the study of chromosome dynamics. *IEEE Trans. Image Process.* 14:1372–1383. http://dx.doi.org/10.1109/TIP.2005.852787

Sakurai-Yageta, M., C. Recchi, G. Le Dez, J.B. Sibarita, L. Daviet, J. Camonis, C. D'Souza-Schorey, and P. Chavrier. 2008. The interaction of IQGAP1 with the exocyst complex is required for tumor cell invasion downstream of Cdc42 and RhoA. *J. Cell Biol.* 181:985–998. http://dx.doi.org/10.1083/jcb.200709076

Sibarita, J.B. 2005. Deconvolution microscopy. *Adv. Biochem. Eng. Biotechnol.* 95:201–243.

Söderberg, O., M. Gullberg, M. Jarvius, K. Ridderstråle, K.J. Leuchowius, J. Jarvius, K. Wester, P. Hydbring, F. Bahram, L.G. Larsson, and U. Landegren. 2006. Direct observation of individual endogenous protein complexes in situ by proximity ligation. *Nat. Methods.* 3:995–1000. http://dx.doi.org/10.1038/nmeth947

Soppina, V., A.K. Rai, A.J. Ramaiya, P. Barak, and R. Mallik. 2009. Tug-of-war between dissimilar teams of microtubule motors regulates transport and fission of endosomes. *Proc. Natl. Acad. Sci. USA.* 106:19381–19386. http://dx.doi.org/10.1073/pnas.0906524106

Steffen, A., G. Le Dez, R. Poincloux, C. Recchi, P. Nassoy, K. Rottner, T. Galli, and P. Chavrier. 2008. MT1-MMP-dependent invasion is regulated by TI-VAMP/VAMP7. *Curr. Biol.* 18:926–931. http://dx.doi.org/10.1016/j.cub.2008.05.044

Sun, F., C. Zhu, R. Dixit, and V. Cavalli. 2011. Sunday Driver/JIP3 binds kinesin heavy chain directly and enhances its motility. *EMBO J.* 30:3416–3429. http://dx.doi.org/10.1038/emboj.2011.229

Tague, S.E., V. Muralidharan, and C. D'Souza-Schorey. 2004. ADP-ribosylation factor 6 regulates tumor cell invasion through the activation of the MEK/ERK signaling pathway. *Proc. Natl. Acad. Sci. USA.* 101:9671–9676. http://dx.doi.org/10.1073/pnas.0403531101

Temkin, P., B. Lauffer, S. Jäger, P. Cimermancic, N.J. Krogan, and M. von Zastrow. 2011. SNX27 mediates retromer tubule entry and endosome-to-plasma membrane trafficking of signalling receptors. *Nat. Cell Biol.* 13:715–721. http://dx.doi.org/10.1038/ncb2252

Tripathy, S.K., S.J. Weil, C. Chen, P. Anand, R.B. Vallee, and S.P. Gross. 2014. Autoregulatory mechanism for dynactin control of processive and diffusive dynein transport. *Nat. Cell Biol.* 16:1192–1201. http://dx.doi.org/10.1038/ncb3063

Wiesner, C., J. Faix, M. Himmel, F. Bentzien, and S. Linder. 2010. KIF5B and KIF3A/KIF3B kinesins drive MT1-MMP surface exposure, CD44 shedding, and extracellular matrix degradation in primary macrophages. *Blood.* 116:1559–1569. http://dx.doi.org/10.1182/blood-2009-12-257089

Williams, K.C., and M.G. Coppolino. 2011. Phosphorylation of membrane type 1-matrix metalloproteinase (MT1-MMP) and its vesicle-associated membrane protein 7 (VAMP7)-dependent trafficking facilitate cell invasion and migration. *J. Biol. Chem.* 286:43405–43416. http://dx.doi.org/10.1074/jbc.M111.297069

Wolf, K., Y.I. Wu, Y. Liu, J. Geiger, E. Tam, C. Overall, M.S. Stack, and P. Friedl. 2007. Multi-step pericellular proteolysis controls the transition from individual to collective cancer cell invasion. *Nat. Cell Biol.* 9:893–904. http://dx.doi.org/10.1038/ncb1616

Yu, X., T. Zech, L. McDonald, E.G. Gonzalez, A. Li, I. Macpherson, J.P. Schwarz, H. Spence, K. Futó, P. Timpson, et al. 2012. N-WASP coordinates the delivery and F-actin-mediated capture of MT1-MMP at invasive pseudopods. *J. Cell Biol.* 199:527–544. http://dx.doi.org/10.1083/jcb.201203025